

This is an Open Access document downloaded from ORCA, Cardiff University's institutional repository: <https://orca.cardiff.ac.uk/id/eprint/150114/>

This is the author's version of a work that was submitted to / accepted for publication.

Citation for final published version:

Schepelmann, Martin , Ranieri, Marianna, Lopez-Fernandez, Irene, Webberley, Thomas S., Brennan, Sarah C. , Yarova, Polina L., Graca, Joao, Hanif, Umar-Khetaab, Müller, Christian, Manhardt, Teresa, Salzmann, Martina, Quasnichka, Helen, Price, Sally A., Ward, Donald T., Gilbert, Thierry, Matchkov, Vladimir V., Fenton, Robert A., Herberger, Amanda, Hwong, Jenna, Santa Maria, Christian, Tu, Chia-Ling, Kallay, Enikö, Valenti, Giovanna, Chang, Wenhan and Riccardi, Daniela 2022. Impaired mineral ion metabolism in a mouse model of targeted calcium-sensing receptor (CaSR) deletion from vascular smooth muscle cells. *Journal of the American Society of Nephrology* 33 (7) , pp. 1323-1340. 10.1681/ASN.2021040585

Publishers page: <http://dx.doi.org/10.1681/ASN.2021040585>

Please note:

Changes made as a result of publishing processes such as copy-editing, formatting and page numbers may not be reflected in this version. For the definitive version of this publication, please refer to the published source. You are advised to consult the publisher's version if you wish to cite this paper.

This version is being made available in accordance with publisher policies. See <http://orca.cf.ac.uk/policies.html> for usage policies. Copyright and moral rights for publications made available in ORCA are retained by the copyright holders.



## **Impaired mineral ion metabolism in a mouse model of targeted calcium-sensing receptor (CaSR) deletion from vascular smooth muscle cells.**

Accepted author manuscript (not proofed, not copyedited; not updated).

The proofed and copyedited published version can be found at:

<https://doi.org/10.1681/ASN.2021040585>

<https://jasn.asnjournals.org/content/early/2022/05/17/ASN.2021040585>

1 Impaired mineral ion metabolism in a mouse model of  
2 targeted calcium-sensing receptor (CaSR) deletion from  
3 vascular smooth muscle cells

---

4  
5 *Martin Schepelmann*<sup>1,2</sup>, *Marianna Ranieri*<sup>3</sup>, *Irene Lopez-Fernandez*<sup>1</sup>, *Thomas S. Webberley*<sup>1</sup>, *Sarah C. Brennan*<sup>1,4</sup>,  
6 *Polina L. Yarova*<sup>1,5</sup>, *Joao Graca*<sup>1,6</sup>, *Umar-Khetaab Hanif*<sup>d</sup>, *Christian Müller*<sup>2</sup>, *Teresa Manhardt*<sup>2</sup>, *Martina*  
7 *Salzmann*<sup>2</sup>, *Helen Quaschnicka*<sup>1</sup>, *Sally A. Price*<sup>6</sup>, *Donald T. Ward*<sup>7</sup>, *Thierry Gilbert*<sup>8</sup>, *Vladimir V. Matchkov*<sup>9</sup>, *Robert*  
8 *A. Fenton*<sup>9</sup>, *Amanda Herberger*<sup>10</sup>, *Jenna Hwong*<sup>10</sup>, *Christian Santa Maria*<sup>10</sup>, *Chia-Ling Tu*<sup>10</sup>, *Enikö Kallay*<sup>2</sup>,  
9 *Giovanna Valenti*<sup>3</sup>, *Wenhan Chang*<sup>10</sup> and *Daniela Riccardi*<sup>1</sup>.

10  
11 1 School of Biosciences, Cardiff University, United Kingdom

12 2 Institute of Pathophysiology and Allergy Research, Medical University of Vienna, Austria

13 3 Department of Biosciences, Biotechnologies and Biopharmaceutics, University of Bari, Italy

14 4 Charles Perkins Centre, University of Sydney, NSW 2006, Australia

15 5 Translational & Clinical Research Institute, Newcastle University Medical School, Newcastle upon Tyne, UK

16 6 AstraZeneca, Macclesfield, Cheshire, United Kingdom

17 7 Division of Diabetes, Endocrinology & Gastroenterology, University of Manchester, Manchester, UK

18 8 Centre for Developmental Biology, University Paul Sabatier, Toulouse, FR

19 9 Department of Biomedicine, Aarhus University, Aarhus 8000, DK

20 10 Department of Medicine, University of California, San Francisco, CA, USA

21  
22 **Running title:** Mineral ion dyshomeostasis in VSMC-CaSR knockout mice

23 **Address correspondence to:**

24  
25 **Wenhan Chang, PhD**

26 University of California San Francisco

27 1700 Owens Street

28 San Francisco CA 94158, USA

29 Phone: (+1) 415-575-0558

30 [Wenhan.Chang@ucsf.edu](mailto:Wenhan.Chang@ucsf.edu)

31  
32 **Daniela Riccardi, PhD**

33 School of Biosciences

34 The Sir Martin Evans Building, Cardiff University

35 Cardiff CF10 3AX, United Kingdom

36 Phone: (44) (0) 29 208 79132

37 [riccardi@cardiff.ac.uk](mailto:riccardi@cardiff.ac.uk)

25 **Martin Schepelmann, PhD**

Institute of Pathophysiology and Allergy Research

Medical University of Vienna

Währinger Gürtel 18-20, Leitstelle 3Q

1090, Vienna, Austria

Phone: (+43) 1 40400 51230

[martin.schepelmann@meduniwien.ac.at](mailto:martin.schepelmann@meduniwien.ac.at)

38 **Significance statement**

39 Chronic kidney disease (CKD) is associated with increased risk of mortality. In CKD, calcium  
40 and phosphate dyshomeostasis are associated with altered expression of the calcium-sensing  
41 receptor (CaSR) in the parathyroid glands and the kidney. The CaSR is also present in the  
42 vasculature, but its contribution to total body mineral ion homeostasis is unknown. Here we  
43 show that selective CaSR ablation from vascular smooth muscle cells (VSMC) leads to  
44 profound mineral ion imbalance in mice. These results demonstrate a hitherto undiscovered  
45 mode of mineral ion regulation outside the parathyroid glands and the kidneys. Alterations in  
46 VSMC-CaSR expression and activity would be expected to contribute to mineral ion imbalance in  
47 CKD.

48 **Abstract**

49 **Background:** Impaired mineral ion metabolism is a hallmark of chronic kidney disease (CKD)  
50 -metabolic bone disorder. It can lead to pathological vascular calcification (VC) and is  
51 associated with an increased risk of cardiovascular mortality. Loss of calcium sensing receptor  
52 (CaSR) expression in vascular smooth muscle cells (VSMCs) exacerbates VC *in vitro*;  
53 conversely, VC can be reduced by CaSR allosteric activators, calcimimetics.

54 **Methods:** To determine the role of the CaSR in VC, we characterized mice with targeted *Casr*  
55 gene knockout (KO) in VSMC ( $^{SM22\alpha}CaSR^{\Delta flox/\Delta flox}$ ).

56 **Results:** VSMC cultured from KO mice calcified more readily than those from control (WT)  
57 mice *in vitro*. However, KO mice did not show ectopic calcifications *in vivo* but a profound  
58 mineral ion imbalance. Specifically, KO mice exhibited hypercalcemia, hypercalciuria,  
59 hyperphosphaturia, and osteopenia, with elevated circulating FGF23, calcitriol (1,25-D<sub>3</sub>), and  
60 PTH levels. Renal tubular, but not vascular  $\alpha$ -Klotho protein expression was increased in KO  
61 mice. The observed phenotype of the KO mice could not be accounted for by altered CaSR  
62 expression in the kidney or the parathyroid glands.

63 **Conclusions:** These results suggest that the VSMC-CaSR directly contributes to total body  
64 mineral ion homeostasis, in addition to the established role of the receptor in the parathyroid-  
65 kidney-bone axis.

## 66 **Introduction**

67 Vascular calcification (VC) is a major complication in chronic kidney disease-metabolic bone  
68 disorder (CKD-MBD) and is an independent predictor of cardiovascular morbidity and  
69 mortality<sup>1</sup>. During VC, pro-contractile vascular smooth muscle cells (VSMC) undergo  
70 osteogenic transdifferentiation<sup>2</sup>. This process is exacerbated by altered mineral ion homeostasis  
71 in CKD-MBD patients<sup>3, 4</sup>. The CaSR is the key regulator of serum ionized calcium levels, *via*  
72 modulation of parathyroid hormone (PTH) secretion by the parathyroid glands (PTG) as well  
73 as Ca<sup>2+</sup> reabsorption in the kidney<sup>5</sup>. Allosteric CaSR activators, calcimimetics, reduce plasma  
74 PTH and Ca<sup>2+</sup> levels, decrease the prevalence of VC in animal studies of CKD<sup>6, 7</sup> and reduce  
75 cardiovascular events in older patients with moderate to severe hyperparathyroidism receiving  
76 hemodialysis<sup>8</sup>. However, the CaSR is also expressed in blood vessels where it may have a direct  
77 protective role against VC. We and others have shown that in VSMC, the CaSR is  
78 vasculoprotective, and that there is an inverse relationship between CaSR expression and VC<sup>9</sup>.  
79 <sup>10</sup>. In uremic rats, administration of calcimimetics protects against VC<sup>9-14</sup>. CaSR expression is  
80 lost in cultured VSMC kept under pro-calcifying conditions *in vitro* and in calcified human  
81 arteries<sup>9, 15</sup> an effect which is, at least in part, restored by calcimimetic treatment<sup>10, 12</sup>. Over-  
82 expression of a “dominant negative” CaSR mutation accelerates calcification of isolated  
83 VSMC, which is prevented by calcimimetics<sup>9</sup>. However, there is a discrepancy between the  
84 preclinical *in vitro* observations and clinical findings about the role of the CaSR in VC. For  
85 instance, CaSR polymorphisms are not determinant of VC or cardiovascular outcomes in renal  
86 transplant patients<sup>16</sup>, suggesting that the protective cardiovascular effects of calcimimetics in  
87 advanced CKD-MBD patients may also be modulated by additional systemic or local factor  
88 like PTH, vitamin D, and FGF23. Thus, the precise contribution of the vascular CaSR to  
89 pathological VC *in vivo* remains to be fully elucidated. To address this question directly, we  
90 studied mice with targeted *Casr* gene ablation in VSMC, in which we have previously

91 demonstrated a significant role of the receptor in the regulation of blood pressure and vascular  
92 tone<sup>17</sup>.

## 93 **Materials and Methods**

94

### 95 **Experimental animals**

96 All animal procedures were approved by local ethical review and conformed with the  
97 regulations of the UK Home Office and/or the Animal Care and Use Committees of all the  
98 participating institutions. VSMC-specific CaSR knock-out mice were produced by breeding  
99 CaSR<sup>flox/flox</sup> mice, which carry 2 loxP sequences flanking exon 7 of the *Casr* gene<sup>18</sup>, with  
100 SM22 $\alpha$  (transgelin)-Cre mice. SM22 $\alpha$  is transiently expressed during embryonic development  
101 in cardiac myocytes and, by mid-gestation, is confined to visceral and vascular SMCs<sup>19</sup>.  
102 Genotyping, husbandry, *etc.* are described in<sup>17, 20</sup>. SM22aCaSR <sup>$\Delta$ flox/ $\Delta$ flox</sup> mice (VSMC-CaSR  
103 knock-out, **KO**) and Cre-negative, CaSR<sup>flox/flox</sup> littermates (called “wild-type”, for the wild-type  
104 CaSR; **WT**) were used for all experiments. Male mice only were used for all experiments,  
105 except for osmolality, soluble CaSR and bone metabolism marker measurements. All mice were  
106 on the same C57Bl/6 genetic background.

### 107 **Culture media**

108 Dulbecco’s modified Eagle medium (DMEM) without CaCl<sub>2</sub>, containing 1 mM phosphate,  
109 (Life Technologies, Grand Island, NY, USA) was supplemented with 1.2 mM CaCl<sub>2</sub>, 50 U/ml  
110 penicillin-streptomycin, 2 mM L-glutamine, 10 % (v/v) fetal bovine serum (FBS), 1 mM Na-  
111 pyruvate and 1 % (v/v) amphotericin B solution (all Life Technologies) was used for the initial  
112 isolation of VSMCs (growth medium). For further culturing, the same medium was used but  
113 with omission of amphotericin B (culture medium). When indicated, the medium was  
114 supplemented with different concentrations of Ca<sup>2+</sup> and inorganic phosphate (Pi) *via* addition  
115 of sterile 1M CaCl<sub>2</sub> solution and inorganic 1M phosphate buffer (NaH<sub>2</sub>PO<sub>4</sub> / Na<sub>2</sub>HPO<sub>4</sub>) pH 7.4.

## 116 **Primary VSMC isolation**

117 VSMC were prepared according to published procedure<sup>21</sup> with modifications. In brief, mice  
118 were killed by cervical dislocation and the thoracic aorta was dissected. Aortas of 2-5 mice of  
119 the same genotype were pooled for one cell isolation and placed in growth medium and cleaned  
120 from the tunica adventitia and connective tissue. Segments of aorta ca. 1 mm in length were  
121 transferred to a culture flask and, after 10 minutes of drying / attaching in a tissue culture  
122 incubator, covered with growth medium and incubated at 37 °C / 95 % relative humidity / 5 %  
123 CO<sub>2</sub> until cells had grown out of the explants (ca. 2-4 weeks). The explants were then removed  
124 by aspiration and the cells were passaged using 0.05 % (v/v) trypsin-ethylenediaminetetraacetic  
125 (EDTA) solution in sterile phosphate-buffered saline, pH 7.4 (PBS) without CaCl<sub>2</sub> and MgCl<sub>2</sub>  
126 (all Life Technologies). Beginning with this passage VSMC culture medium was used instead  
127 of growth medium. Medium was changed every 3-4 days. Cells were used for experiments at  
128 passages 2-6. See **Figure S1** for a photograph array of the procedure.

## 129 **Immunohistochemistry**

130 Mouse organs were fixed by immersion in 4 % (w/v) paraformaldehyde (PFA) in PBS for 4  
131 hours and 4 µm paraffin sections were cut and rehydrated according to standard protocols.  
132 Immunostainings were carried out to detect CaSR (1:500, MA1-934, Thermo Scientific,  
133 Loughborough, UK), TRPV5 (1:400, Alomone Labs, Jerusalem, Israel), Calbindin D-28k  
134 (1:3000, Sigma-Aldrich, Gillingham, UK), and PMCA 1/4 (1:100, Santa Cruz Biotechnology,  
135 Santa Cruz, USA). These immunostainings were carried out using a Ventana XT autostainer  
136 and Omnimap<sup>TM</sup> DAB reagents (Ventana, Tucson, USA). Hematoxylin (Clin-Tech,  
137 Guildford, UK) was used to counterstain the tissue sections, which were then dehydrated in  
138 ethanol, cleared in xylene, and mounted using Hystomount (TAAB Labs, Aldermaston, UK) or  
139 Fluoromount G (Thermo Fisher). Cyp27b1 and α-Klotho protein in aortas was detected using  
140 rabbit anti-Cyp27b1 (1:500, LSBio, Seattle, USA) and rabbit anti-klotho (1:200, Abcam)



141 antibodies, respectively. Antigen retrieval was performed by incubation for 20 min in 10 mM  
142 citrate buffer pH 6 in a steamer. Bound antibodies were visualized using the Dako Envision+  
143 HRP rabbit kit (Agilent, Santa Clara, USA), nuclei were counterstained using Haematoxylin  
144 and mounted in Fluoromunt G. Tissue slides were scanned using a Scanscope® scanner (Aperio  
145 Technologies Incorporated, Vista, USA) or TissueFAXS Hard- and Software (TissueGnostics  
146 GmbH, Vienna, Austria). Quantitative evaluation of immunohistochemical stainings was  
147 performed using ImageJ<sup>22, 23</sup>, where % positive cells / positive area was counted after manual  
148 thresholding. For the aorta sections, mean color value for endothelium and smooth muscle layer  
149 were measured by subtracting the values of the negative controls for each aorta (IgG control)  
150 from the positively stained sections.

### 151 **Immunofluorescence**

152 Dissected organs were fixed by immersion in 4 % (w/v) PFA in PBS for 4 hours and then  
153 washed in PBS and stored in 30 % (w/v) sucrose in PBS at 4 °C for cryosections or dehydrated  
154 and paraffin embedded for paraffin sections. For cryosections, tissues were embedded in  
155 optimal cutting temperature compound (TissueTek OCT, Sakura-Finetek, Alphen aan den Rijn,  
156 NL) on dry ice and 8-10 µm sections were prepared using a cryo-microtome (Leica 2300L,  
157 Leica microsystems, Milton Keynes, UK). Rehydrated sections were incubated for 10 minutes  
158 in 50 mM NH<sub>4</sub>Cl in PBS and then were antigen retrieved in 10 mM citrate buffer pH 6 for 15  
159 minutes in a steamer followed by 5 minutes in 1 % sodium dodecyl sulphate (SDS) in PBS.  
160 Non-specific antibody binding was prevented by incubation in 1 % (w/v) BSA + 0.1 % (v/v)  
161 Tween 20 in PBS (blocking buffer) for 1 hour at room temperature. The CaSR was labelled by  
162 incubating the sections overnight with a rabbit-derived polyclonal antibody (1:100; AnaSpec,  
163 53286, Fremont, CA, USA) or a mouse derived monoclonal antibody (1:500, clone 5C10,  
164 Abcam) in blocking buffer. Negative controls were performed by omission of the primary  
165 antibodies or replacement with an isotype control of rabbit IgG (Abcam). After washing in PBS,

166 primary antibody binding was visualized using appropriate Alexa Fluor fluorescence-dye  
167 coupled secondary anti IgG antibodies in a dilution of 1:500 in blocking buffer. High  
168 background was quenched by incubation of the sections in 0.2 mM Sudan Black B in 70 %  
169 ethanol for 10 minutes after the secondary antibody<sup>24</sup>. Nuclei were counterstained with Hoechst  
170 34580 and slides were mounted using ProLong Gold® (all Life Technologies).

### 171 ***In vitro* calcification assays**

172 Cells were seeded in 24-well plates and were grown to 100 % confluency. The medium was  
173 then changed to growth medium supplemented with various CaCl<sub>2</sub> concentrations as specified  
174 in the results section. For induction of calcification, Pi (in the form of 1 M Na-phosphate buffer  
175 pH 7.4) were added to the culture medium. Cells were left in culture for 10 days and then fixed  
176 for 15 minutes in 4 % (w/v) PFA at room temperature. The amount of calcification was  
177 visualized by staining with 2 % alizarin red S (w/v) in water, pH 4.3, as described<sup>25</sup>. For  
178 quantification, after the incubation period, the cells were washed twice in PBS for and deposited  
179 calcium was extracted by decalcifying overnight in 0.6 N HCl at 37 °C. Eluted Ca<sup>2+</sup>  
180 concentration was measured using the o-cresolphthalein complexone method<sup>26, 27</sup> and  
181 normalized against total protein concentration of the lysed cells (Pierce BCA assay; Thermo  
182 Fisher Scientific).

### 183 ***Ex vivo* calcification of aortic explants**

184 The assay was performed as described elsewhere<sup>28</sup>. In brief, aortas were dissected as described  
185 for the primary VSMC isolation. After cleaning the aortas from tunica adventitia, the  
186 endothelial layer was destroyed by stretching the tissue over the whole length. The vessel was  
187 then cut into 3-4 pieces of approximately equal length (5–8 mm). The pieces were incubated  
188 for 5 days in growth medium supplemented with varying of CaCl<sub>2</sub> concentrations (1.2–2.5 mM)  
189 and 3 mM inorganic phosphate, similarly to the VSMC calcification assays. Ca<sup>2+</sup> concentrations  
190 were measured by o-cresolphthalein complexone method as described above and normalized

191 against the weight of the explants. Typical explant weights varied between 1.0 and 5.0 mg.  
192 Cryosections of 4 % (w/v) PFA fixed WT and KO aortas were stained for calcifications using  
193 Alizarin Red S as described above.

#### 194 **Parathyroid isolation and *ex vivo* PTH secretion**

195 The *ex vivo* PTH-secretion assay in cultured mouse PTGs was adapted from<sup>29</sup>. Briefly, two  
196 mouse PTGs cleaned from surrounding tissues were submerged in a micro-droplet (10  $\mu$ l) of  
197 secretion medium [SM, MEM Eagles with Earle's balanced salts supplemented with 0.5 mM  
198 Mg, 0.2 % bovine serum albumin, and 20 mM HEPES (pH 7.4)] and placed in the center of a  
199 13 mm track-etched (0.1  $\mu$ m pore) polycarbonate (PC) membrane, floating on a large drop (0.5  
200 ml) of ice-cold SM supplemented with 3.0 mM  $\text{Ca}^{2+}$ . When all glands for the same experiment  
201 were dissected out, the PC membranes carrying the glands were transferred onto fresh drops of  
202 37 °C SM containing 0.5 mM  $\text{Ca}^{2+}$  and equilibrated for ~45 minutes. Afterwards, the membrane  
203 with each pair of glands was transferred sequentially to a fresh drop (500  $\mu$ l) of SM at 37 °C,  
204 increasing the  $\text{Ca}^{2+}$  concentration in the medium from 0.5 to 3.0 mM with 60 min for each  
205 concentration and a fresh medium change midway (at 30 minutes). Intact PTH released into the  
206 culture media was determined by ELISA (Quidel, San Diego, USA) in duplicate and used to  
207 calculate the rate of PTH release. For  $\text{Ca}^{2+}$  set-points, rates of PTH release were normalized to  
208 the rate at 0.5 mM  $\text{Ca}^{2+}$  and plotted against the  $\text{Ca}^{2+}$  concentration, and the PTH set-points (=  $\text{EC}_{50}$ )  
209 were deduced from the curve as the  $\text{Ca}^{2+}$  concentration which inhibits 50 % of the  $\text{Ca}^{2+}$ -  
210 suppressible PTH release.

#### 211 **Microcomputed tomography ( $\mu$ CT)**

212  $\mu$ CT was performed on distal femur for trabecular (Tb) bone and tibio-fibular junction (TFJ)  
213 for cortical (Ct) bone as described<sup>29</sup>. Briefly, femurs and tibiae fixed in 10 % phosphate-  
214 buffered formaldehyde (PBF) were scanned by a SCANCO vivaCT 100 scanner (SCANCO  
215 Medical AG, Basserdorf, Switzerland) with 10.5  $\mu$ m voxel size and 55 kV X-ray energy. For

216 Tb bone in the distal femoral metaphysis, 100 serial cross-sectional scans (1.05 mm) of the  
217 secondary spongiosa were obtained from the end of the growth plate extending proximally. For  
218 Ct bone, 100 serial cross-sections (1.05 mm) of the tibia were obtained from the TFJ extending  
219 proximally. A threshold of 420 mg hydroxyapatite (HA)/mm<sup>3</sup> was applied to segment total  
220 mineralized bone matrix from soft tissue. Linear attenuation was calibrated using a  $\mu$ CT HA  
221 phantom.  $\mu$ CT image analysis and 3D reconstructions were done using the manufacturer's  
222 software to obtain the following structural parameters: Tb tissue volume (Tb.TV), Tb bone  
223 volume (Tb.BV), Tb.BV/TV ratio, Tb number (Tb.N), Tb connectivity density (Tb.CD), Tb  
224 thickness (Tb.Th), Tb spacing (Tb.Sp), Ct tissue volume (Ct.TV), and Ct thickness (Ct.Th).

### 225 **Nephron count**

226 One kidney per adult animal (16 weeks) was removed, decapsulated and immersed in 6M HCl  
227 at 37°C for 35 minutes. After several washes with tap water, the macerated kidney was stored  
228 at 4°C overnight. The tissue was homogenized with a glass-stirring rod and transferred to a 50  
229 ml volumetric flask. Tap water was added to adjust the volume and the tubules and glomeruli  
230 suspension was then ready for nephron counting. One 0.5 ml aliquot was taken and deposited  
231 onto a glass slide with a millimeter mesh lattice to count the number of glomeruli. The total  
232 number of nephrons per kidney was calculated using the mean of 3 to 4 counts.

### 233 **Tissue preparation for Western blot and RT-qPCR experiments**

234 Mouse kidney slices were prepared as previously described<sup>30</sup>. In brief, WT and KO mice were  
235 euthanized by cervical dislocation. Kidneys were quickly removed and about 500  $\mu$ m sections  
236 were made. Sectioned kidneys were equilibrated for 10 min in a specific kidney-slice buffer  
237 that contained 118 mM NaCl, 16 mM HEPES, 17 mM Na-HEPES, 14 mM glucose, 3.2 mM  
238 KCl, 2.5 mM CaCl<sub>2</sub>, 1.8 mM MgSO<sub>4</sub>, and 1.8 mM KH<sub>2</sub>PO<sub>4</sub> (pH 7.4) at 37°C. For Western  
239 blotting experiments, sections were then homogenized with a mini-potter in ice-cold kidney-  
240 slice buffer and Halt™ protease and phosphatase inhibitor Cocktail (Thermo Fisher, Rockford,

241 USA). Suspensions were centrifuged at 12,000 x *g* for 10 min at 4°C, and supernatants were  
242 loaded on acrylamide gels. Bones were prepared from hind-leg bones (femur, tibia and fibia)  
243 after cleaning of the surrounding connective tissue. After cleaning of the aortas from the tunica  
244 adventitia, the vessel was cut into 3-4 pieces, which were then processed accordingly.  
245 For RT-PCR experiments, total RNA was extracted from kidneys, aorta and bones using Trizol  
246 reagent according to the manufacturer's instructions (Invitrogen, Life Technologies, Monza,  
247 Italy).

### 248 **Gel Electrophoresis and Immunoblotting**

249 Proteins were separated on 8-13 % bis-tris acrylamide gels under reducing conditions. Protein  
250 bands were electrophoretically transferred onto Immobilon-P membranes (Millipore Corporate  
251 Headquarters, Billerica, USA) for Western blot analysis, blocked in TBS-Tween-20 containing  
252 3 % bovine serum albumin (BSA) and incubated with primary antibodies overnight.

253 Antibodies: polyclonal rabbit anti-CaSR (AnaSpec, this antibody had previously been  
254 determined to be most suitable for mouse tissue<sup>31</sup>), polyclonal rabbit anti-AQP2 (raised against  
255 20-amino acids at the N-terminal, custom made from the polyphosphorylated region of rat  
256 AQP2)<sup>32</sup>, polyclonal rabbit anti-AQP2-pS256 (a gift from Peter Deen)<sup>33</sup>, polyclonal rabbit anti-  
257 AQP2-pS261 (Novus Biologicals, Littleton, Colorado, USA), polyclonal antibody against  
258 NaPi2a (Alpha Diagnostic Intl. Inc, San Antonio, Texas, USA), polyclonal rabbit anti-Klotho  
259 (Abcam, Cambridge, UK), monoclonal mouse anti-NCC (StressMarq Biosciences Inc.,  
260 Victoria, CDN), polyclonal rabbit anti-β-actin (Cell Signaling Technology, Leiden, NL) and  
261 rabbit antibodies raised against the last 10 C-terminal amino acids (C-GANANRKFLD) of the  
262 E subunit of the V-ATPase (a gift from Dr Dennis Brown, Harvard Medical School, Boston,  
263 MA, USA). Secondary goat anti-rabbit or goat anti-mouse horseradish peroxidase-coupled  
264 antibodies were obtained from Santa Cruz Biotechnologies (Tebu-Bio, Milan, IT). Membranes  
265 were developed using Super Signal West Pico Chemiluminescent Substrate (Pierce, Rockford,

266 USA) with Chemidoc System (Bio-Rad Laboratories, Milan, Italy). Densitometry analysis was  
267 performed using Image Lab from Bio-Rad Laboratories, Inc. (Hercules, California, USA).

## 268 **Real-Time PCR**

269 Real-Time PCR experiments were performed to measure the relative expression of mRNA from  
270 WT and KO mouse kidneys, aorta, and bone. Total RNA was extracted using Trizol (Invitrogen,  
271 Life Technologies, Monza, Italy). Reverse transcription was performed on 1 µg of total RNA  
272 using SuperScript VILO Master Mix (Invitrogen, Life Technologies, Monza, Italy). Real-time  
273 PCR amplification was performed using TaqMan® Fast Advanced Master Mix with Aqp2 (ID  
274 number: Mm00437575\_m1), CaSR (ID number: Mm00443375\_m1), α-Klotho (ID number:  
275 Mm00502002\_m1), NaPi2a (ID number: Mm00441450\_m1), Tagln or Sm22α (ID number:  
276 Mm00441661\_g1), FGF23 (ID number: Mm00445621\_m1) and CYP27B1 or 1α-hydroxylase  
277 (ID number: Mm01165918\_g1) assay, using GAPDH (ID number: Mm99999915\_g1) and 18S  
278 (ID number: Hs99999901\_s1) assay as housekeeping genes (Applied Biosystem, Life  
279 Technologies, Monza, Italy) in a StepOne Real-Time PCR System (Applied Biosystem, Life  
280 Technologies, Monza, Italy). Results were calculated according to the  $\Delta\Delta C_t$  method as relative  
281 expression to the average gene expression in the WT samples and then calculated as fold  
282 changes via  $2^{-\Delta\Delta C_t}$ .

## 283 **Blood and urine collection, metabolic cages**

284 Post-mortem blood collection from animals after neck dislocation was performed *via* cardiac  
285 puncture or retro-orbitally. Blood collection from live animals was performed *via* tail nick, as  
286 described<sup>34</sup>. K-EDTA, Na-heparin plasma and serum were collected in respective tubes (BD  
287 Biosciences, Oxford, UK). The blood was then centrifuged at 2,000 x g for 10 minutes and the  
288 supernatant stored at -80 °C. For urine collection, mice were weighed and transferred to  
289 metabolic cages (Tecniplast, Buguggiate, IT) and then left for 48 hours to allow them to  
290 acclimatize to the new environment. Mouse weight, food and water intake, as well as feces and

291 urine production were recorded over a period of 4 days. Samples from day 3 and 4 were then  
292 used for urine analysis and the results for both days were averaged. Urine was stored at -80 °C  
293 for further analysis.

## 294 **Blood and urine analysis**

295 Commercially available assays were used to measure plasma concentrations of Fetuin A (R&D  
296 Systems, Abingdon, UK), pyrophosphate (Abcam), FGF 23 (Kainos Laboratories, Tokyo,  
297 Japan), 1–84 PTH (Immutopics, San Clemente, USA), calcitriol (1,25-D<sub>3</sub>) (Immunodiagnostic  
298 Systems, Tyne & Wear, UK), P1NP (Immunodiagnostic Systems), and TRAcP5b  
299 (Immunodiagnostic Systems), as well as serum concentration of soluble CaSR / N-terminal  
300 CaSR fragment (Elabscience, Wuhan, CN), and  $\alpha$ -Klotho (cloud Clone Corp., Wuhan, CN).  
301 Concentrations of electrolytes were analyzed using a Roche modular P analyzer (Roche  
302 diagnostics) or, as were urea, creatinine, uric acid, glucose, and protein, by a commercially  
303 available clinical pathology service (MRC Harwell, Oxford, UK). Serum osmolality was  
304 measured using an Osmomat 30 (Gonotec, Berlin, DE) freezing point depression osmometer.  
305 Electrolyte concentrations for urine are reported as ion:creatinine ratio (abbreviated as ion:Cr),  
306 other clinical urine biomarkers (creatinine, total protein, urea and uric acid) are reported as  
307 excreted amount per day and total body weight (TBW). Urine osmolality was measured using  
308 a VAPRO® vapor pressure osmometer 5520 Wescor Inc., (Puteaux, France). Urine pH was  
309 measured using litmus paper with a range of pH between 2.0 and 9.0 (Macherey-Nagel, Düren,  
310 Germany). For urine precipitated analysis, 20  $\mu$ l of urine were placed on the glass slide and  
311 covered with a coverslip. Samples were studied with phase contrast microscopy and analyzed  
312 qualitatively. Urinary AQP2 excretion was measured by ELISA as previously described<sup>35, 36</sup>.

## 313 **Statistical Analysis**

314 All statistical analyses were performed using GraphPad Prism 8 (GraphPad Software, La Jolla,  
315 CA, USA). Statistical sample size is reported as N (number of separate experiments / biological

316 repeats) over n (technical repeats per sample, where applicable). Data are generally presented  
317 as mean  $\pm$  SD, except for RT-qPCR data, which are shown as median  $\pm$  interquartile range.

318 A difference of  $p < 0.05$  was considered statistically significant. The employed statistical tests  
319 and significance levels are specified in the respective results sections or in the figure legends.

## 320 **Results**

### 321 **CaSR ablation induces calcification of VSMC *in vitro* but not *ex vivo* or *in vivo*.**

322 Effectiveness of CaSR ablation from VSMC of *SM22 $\alpha$* CaSR <sup>$\Delta$ lox/ $\Delta$ lox</sup> mice, at the molecular and  
323 functional levels, had already been confirmed previously<sup>17, 37</sup>. To test directly whether CaSR  
324 ablation prompts VSMCs to calcify, VSMC isolated from WT and KO mice were cultured in  
325 rising concentrations of Ca<sup>2+</sup> (0.8–2.2 mM) and inorganic phosphate (Pi, 2–3 mM), spanning  
326 the (patho)physiological range. WT VSMC showed no calcification at 2 mM Pi at any Ca<sup>2+</sup>  
327 concentration, while at 3 mM Pi, calcification was seen at  $\geq 1.6$  mM Ca<sup>2+</sup>. In VSMC derived  
328 from KO aortae, calcification was significantly greater, and was already observed in 2 mM Pi  
329 at 1.6 mM Ca<sup>2+</sup> or in 3 mM Pi at 1.2 mM Ca<sup>2+</sup> (**Figure 1A**). Ca<sup>2+</sup> incorporation in VSMC was  
330 Ca<sup>2+</sup>-concentration dependent and was markedly more pronounced in VSMC from KO than in  
331 those from WT mice (**Figure 1B**). Furthermore, VSMC from WT and KO mice were cultured  
332 in 3 mM Pi and only 1.2 mM Ca<sup>2+</sup>, so as to not saturate CaSR-activation, but in combination  
333 with 10 nM of the calcimimetic R-568. R-568 reduced calcium incorporation only in WT but  
334 not KO VSMC when compared to vehicle control (**Figure 1C**). Together, these results  
335 confirmed that the CaSR protects *in vitro* VSMC calcification.

336 Based on these observations, we had expected the KO mice to develop calcification in their  
337 blood vessels. However, there was no evidence of increased *in vivo* Ca<sup>2+</sup> incorporation in the  
338 aortas of three-month-old KO mice compared to age matched WT controls. *Ex vivo* whole aortic  
339 explants from both six-month-old KO and WT mice, kept for ten days in 3 mM Pi and 1.8 mM



340  $\text{Ca}^{2+}$  did not show any traceable calcification by alizarine red staining (**Figure S2**) and/or  $\mu\text{CT}$   
341 (data not shown). Finally, as shown previously, aortas from up to 12-month-old WT and KO  
342 mice were histologically comparable and devoid of calcium deposits<sup>17</sup>.

343

344 *SM22 $\alpha$*  **CaSR $\Delta\text{flox}/\Delta\text{flox}$  mice exhibit impaired mineral ion homeostasis and alterations**  
345 **in calciotropic and phosphotropic hormones.**

#### 346 *Blood biochemistry*

347 Measurement of blood parameters, as shown in **Table 1**, showed moderate hypercalcemia and  
348 elevated plasma FGF23, PTH and 1,25-D<sub>3</sub> levels in 3-month-old mice. FGF23 and  $\text{Ca}^{2+}$  levels  
349 were also measured and found to be elevated in 18-month-old mice (**Table S1**) indicating that  
350 the mineral ion imbalance persists throughout the lifespan of the KO mice, without any apparent  
351 detrimental impact on their health. Serum  $\alpha$ -Klotho-levels were comparable between both  
352 genotypes, at 3- and 18-months of age, although older mice had higher mean  $\alpha$ -Klotho-levels  
353 than the younger ones.

354 Plasma Pi concentrations were reduced in 3-month-old KO compared to WT animals while  
355  $\text{Na}^+$ ,  $\text{K}^+$ ,  $\text{Cl}^-$  and  $\text{Mg}^{2+}$  levels, and the levels of the physiological inhibitors of calcification,  
356 inorganic pyrophosphate (PPi) and Fetuin A were comparable between genotypes. Serum  
357 albumin levels were slightly decreased (pointing also towards a higher proportion of free  
358 ionized  $\text{Ca}^{2+}$  levels) while alkaline phosphatase (ALP) levels were increased in KO animals.  
359 Kidney function and hydration appeared to be normal in KO mice as urea and blood urea  
360 nitrogen (BUN), as well as hematocrit, did not differ from those of WT animals, while serum  
361 creatinine was slightly reduced in KO animals (**Table 1**). Serum osmolality assessed in the 18-  
362 month-old animals was unchanged between the two genotypes (**Table S1**). We also detected  
363 no difference in the concentration of “soluble” CaSR or rather N-terminal CaSR fragment  
364 between the genotypes in sera of 18-month-old animals (**Table S1**) which was comparable to

365 the level seen in serum of a 14-month-old non-genetically modified control (Ctrl) mouse.  
366 “Soluble” CaSR was around the lowest detection limit in sera of 3-month-old animals (**Figure**  
367 **S8**). These results exclude an antagonistic or hormonal effect of the truncated CaSR (encoded  
368 by exons 2-6) as the cause for the observed phenotype.

369

### 370 *Metabolism, urine and organ weight*

371 Urinary Ca<sup>2+</sup>:Cr and Pi:Cr levels of KO were strongly elevated compared to WT animals (7.2-  
372 fold and 2.9-fold respectively), while Na<sup>+</sup>:Cr, K<sup>+</sup>:Cr, Cl<sup>-</sup>:Cr and Mg<sup>2+</sup>:Cr, creatinine, total  
373 protein, urea, uric acid, and glucose excretion ratios were comparable between the genotypes  
374 (**Table 2**). No differences in food consumption or fecal output were observed between  
375 genotypes. Water consumption and urine excretion were non-significantly elevated in KO mice  
376 compared to WT (**Table 2, Figure S3**).

377

### 378 *Mineral ion and hormonal imbalance seen in <sup>SM22 $\alpha$</sup> CaSR $\Delta$ flox/ $\Delta$ flox mice is not a direct* 379 *consequence of altered gene/protein expression in the vasculature (aorta).*

380 The observed phenotype points to a profound mineral ion dyshomeostasis in KO mice. We  
381 therefore investigated the expression of  $\alpha$ -Klotho and 1 $\alpha$ -hydroxylase since they are powerful  
382 regulators of mineral ion metabolism. mRNA expression of  $\alpha$ -Klotho, *Cyp27b1*, and the smooth  
383 muscle marker *sm22 $\alpha$*  were unchanged between WT and KO animals. CYP27B1 and  $\alpha$ -Klotho  
384 protein expression levels were comparable between genotypes in both the endothelium and  
385 smooth muscle layers of the aorta (**Figure 2**). The cause of the observed mineral ion and  
386 hormonal imbalance in KO mice must therefore lie elsewhere.

387

388 *SM22a***CaSR** <sup>$\Delta$ flox/ $\Delta$ flox</sup> mice exhibit altered expression of renal  $\alpha$ -Klotho and of Ca<sup>2+</sup> and Pi  
389 transport proteins.

390 Renal expression of  $\alpha$ -Klotho protein was significantly increased while that of the proximal  
391 tubule Na<sup>+</sup>-dependent Pi transporter NaPi2a was significantly decreased in the kidneys of KO  
392 mice. The number of vitamin D receptor positive cells over whole kidney sections as  
393 determined by semi-quantitative immunohistochemistry analysis was comparable between  
394 genotypes, as was the mRNA expression of *Cyp27b1* (**Figure 3 and Figure S4**). The elevated  
395 plasma levels of 1,25-D<sub>3</sub> seen in KO mice could not be explained by the unchanged CYP27B1  
396 protein expression in the kidney, which was comparable between genotypes (**Figure S5**),  
397 indicating extrarenal sources of 1,25-D<sub>3</sub>. In supporting the action of 1,25-D<sub>3</sub> to increase urinary  
398 Ca<sup>2+</sup> reabsorption<sup>38</sup>, the expression of the epithelial Ca<sup>2+</sup> channel TRPV5, the cytosolic Ca<sup>2+</sup>  
399 buffer calbindin D28K, and the basolateral plasma membrane Ca<sup>2+</sup>-ATPase (PMCA) was  
400 significantly increased in kidneys from KO compared to WT mice, as indicated by the larger  
401 area where staining intensities were above the threshold level (**Figure 3**).

402 Next, we confirmed that CaSR ablation from VSMC did not yield altered CaSR expression or  
403 gross anatomical changes in the kidney which could account for the observed phenotype. Renal  
404 CaSR mRNA and protein expression and distribution pattern (**Figure 3, Figure S6**) were all  
405 comparable between genotypes. There were no histomorphological differences between the  
406 kidneys of WT and KO mice of comparable age (**Figure S6A, B**). Kidney weights were  
407 comparable between WT and KO animals, both at 6 and 18 months of age (**Table S2**), as were  
408 nephron numbers (WT 30.54±5.21 vs KO 31.63±4.80 nephrons/mg kidney, mean±SD, N=7).  
409 Other organ weights (liver, stomach, spleen) were similar between genotypes, except for the  
410 hearts of 18-month-old KO animals, which were slightly heavier than those of age-matched WT  
411 animals (**Table S2**).

412

413 ***Urinary crystals, dilution and aquaporin expression levels of  $SM22aCaSR^{\Delta flox/\Delta flox}$  mice.***

414 The observed hypercalciuria and hyperphosphaturia could promote renal stone formation.  
415 While overt nephrolithiasis or nephrocalcinosis were not detected by histopathology, we did  
416 observe micro crystals in the urine of KO, but not WT animals (**Figure 4A**). Urine of KO mice  
417 had significantly reduced osmolality and pH compared to WT controls (**Figure 4**). The  
418 expression of the apical thiazide-sensitive  $Na^+-Cl^-$  cotransporter (NCC) and of the V-type  $H^+$   
419 ATPase were significantly increased in KO mouse kidneys, potentially leading to increased  
420 NaCl reabsorption and urine acidification respectively. Accordingly, the expression of the  
421 aquaporin-2 water channel (total AQP2) was significantly reduced in the kidneys of KO mice  
422 at both the mRNA and protein levels (**Figure S4** and **Figure 4F**). Specifically, the expression  
423 of the proteasome-sensitive phosphorylated form of AQP2, pS261<sup>39</sup>, was upregulated while the  
424 active, vasopressin-stimulated pS256-AQP2<sup>35</sup> was downregulated in KO mice (**Figure 4G, H**),  
425 indicating a decreased amount of functional AQP2 resulting in decreased renal concentrating  
426 ability. In addition, urinary excretion of AQP2 was increased in KO animals (**Figure 4I**),  
427 pointing towards a higher degree of AQP2 degradation. Overall, KO mice had reduced urine  
428 concentrating ability, possibly as compensation to prevent kidney stone formation.

429

430 ***Hyperparathyroidism of  $SM22aCaSR^{\Delta flox/\Delta flox}$  mice is neither due to altered CaSR expression,***  
431 ***nor function, in the PTG.***

432 VSMC-CaSR KO mice exhibit hypercalcemia and mild hyperparathyroidism (to reiterate,  
433 plasma total  $Ca^{2+}$ : 2.28 mmol / l vs. 2.94 mmol / l and PTH 151.7 vs. 256.6 pg/ml, WT vs. KO,  
434 see **Table 1**). To investigate whether the observed phenotype was due to partial ablation of the  
435 parathyroid CaSR, possibly through *SM22a* promoter leakage, we characterized CaSR  
436 expression and PTG function in the KO animals. PTGs from WT and KO animals were  
437 comparable in size and morphology (**Figure 5A**), as was the glands' CaSR expression (**Figure**

438 **5B and C**). Similarly, isolated PTGs had overlapping PTH secretion curves in response to rising  
439 levels of extracellular  $\text{Ca}^{2+}$  for both genotypes with identical  $\text{IC}_{50}$  values of  $\sim 1.1 \text{ mM Ca}^{2+}$ <sub>o</sub>  
440 (**Figure 5D**). Thus, the profound changes in mineral ion homeostasis seen in KO animals cannot  
441 be accounted for by altered CaSR expression, or function, in the PTGs.

442

443 *SM22aCaSR<sup>Δflox/Δflox</sup> mice exhibit elevated bone FGF23 levels and osteopenia.*

444 The increased circulating levels of the phosphaturic hormone FGF23 are, at least in part, of  
445 skeletal origin, as FGF23 mRNA expression levels were increased in bones of KO mice (**Figure**  
446 **S7**). In contrast, FGF23 mRNA was undetectable in blood vessels of both genotypes (no  
447 amplification).

448 Micro-computerized tomography ( $\mu\text{CT}$ ) on hind-leg bones of 3-month-old WT and KO mice  
449 revealed that especially trabecular bone quality was significantly reduced in KO animals  
450 compared to WT (**Table 3, Figure S7**). These findings are in line with a significant increase in  
451 plasma levels of the bone resorption marker tartrate-resistant acid phosphatase 5b (TRAcP5b)  
452 in KO compared to WT animals, while the bone formation marker procollagen type 1 (P1NP)  
453 was comparable in both genotypes (**Figure S7**).

## 454 **Discussion**

455 Our data suggest that the CaSR protects VSMC from calcification *in vitro*, though loss of the  
456 VSMC-CaSR is apparently unable to induce detectable VC *in vivo*. Our mouse model further  
457 demonstrated that the VSMC-CaSR contributes directly to the regulation of mineral ion  
458 homeostasis, possibly by direct control of FGF23 and 1,25-D3 production / secretion, or  
459 indirectly through influencing the calcium-sensing or hormonal resistance in calciotropic  
460 organs. Most likely, the phenotype of the *SM22aCaSR<sup>Δflox/Δflox</sup>* mouse is the result of a  
461 combination of disturbances acting together (**Figure 6**).

462 **Vascular and VSMC calcification**

463 VC is an independent predictor of cardiovascular morbidity and mortality in CKD-MBD  
464 patients<sup>40, 41</sup>. Previous observations in cultured human and bovine VSMC<sup>9</sup> indicated a direct  
465 role for the CaSR in preventing VSMC calcification / VC, which is substantiated by our findings  
466 on the effect and ability of CaSR ablation and calcimimetics to enhance and prevent VSMC  
467 calcification *in vitro*, respectively. These observations suggest that calcimimetics used  
468 clinically to treat patients with end-stage renal disease may reduce VC by directly targeting the  
469 vascular CaSR in addition to its action of improving mineral ion metabolism. However, the  
470 absence of VC in the aortae of KO mice *in vivo*, despite the animals' hypercalcemia, suggests  
471 that loss of CaSR expression is not sufficient to drive pathological VC.

472 An increase in 1 $\alpha$ -hydroxylase expression in the vasculature promotes VC<sup>42</sup> but 1 $\alpha$ -hydroxylase  
473 expression in the aortas of *SM22a**CaSR* $\Delta$ *fl**ox*/ $\Delta$ *fl**ox* mice is not affected. High serum Pi levels are  
474 associated with greater prevalence of VC in patients with moderate CKD<sup>43</sup> whereas the  
475 *SM22a**CaSR* $\Delta$ *fl**ox*/ $\Delta$ *fl**ox* were hypophosphatemic. Together with unchanged fetuin A and  
476 pyrophosphate (PPi) levels, potentially in combination with factors such as reduced vascular  
477 resistance in these animals<sup>17</sup>, this may explain the lack of *in vivo* VC of *SM22a**CaSR* $\Delta$ *fl**ox*/ $\Delta$ *fl**ox* mice.

478 **Mineral ion metabolism imbalance**

479 In addition to the previously described phenotype of reduced vascular contractility<sup>17</sup> and the  
480 changes in VSMC calcification behavior discussed above, we found that the *SM22a**CaSR* $\Delta$ *fl**ox*/ $\Delta$ *fl**ox*  
481 mice also showed dysregulated mineral ion imbalance, manifesting in hypercalcemia,  
482 hypophosphatemia, hypercalciuria, hyperphosphaturia, and elevated FGF23, PTH, and 1,25-D<sub>3</sub>  
483 levels, together with increased bone resorption that is probably due to the chronically elevated  
484 PTH levels.

485 ***The phenotype is a direct consequence of VSMC-specific CaSR deletion***

486 CaSR expression and / or function in PTG and kidney was not affected in the  $SM22aCaSR^{\Delta flox/\Delta flox}$   
487 mice. Indeed, the phenotype of these mice cannot be explained by off-target CaSR deletion  
488 induced by our knock-out strategy, as constitutive or calcitropic organ specific CaSR deletion  
489 have very different phenotypes (**Table 4**). The global CaSR knock-out mouse exhibits severe  
490 hyperparathyroidism, growth retardation, and rarely lives longer than a few weeks<sup>44</sup> while the  
491  $SM22aCaSR^{\Delta flox/\Delta flox}$  mice grow normally and have a normal lifespan. Using our strategy ( $\Delta$ exon  
492 7), targeted deletion of the CaSR from the PTG was shown to induce a severe phenotype of  
493 hypercalcemia and hyperparathyroidism (~20-fold higher compared to controls)<sup>18</sup>, along with  
494 PTGs whose secretion are totally unresponsive to rising  $Ca^{2+}$  concentrations<sup>45</sup>. The PTGs of the  
495  $SM22aCaSR^{\Delta flox/\Delta flox}$  mice however were as responsive to extracellular  $Ca^{2+}$  as those from WT  
496 mice. A similar strategy ( $\Delta$ exon 3) was used to specifically delete the CaSR from the kidney,  
497 and these mice exhibit normal serum biochemistries and hypocalciuria<sup>46</sup>. Off-target effects of  
498 the truncated amino terminus of the CaSR are also highly unlikely, given that circulating levels  
499 of the (truncated) receptor were extremely low which would not be expected to interfere with  
500 the millimolar extracellular  $Ca^{2+}$  concentration, and that the residual truncated protein is by  
501 itself inactive and does not hinder the function of the native CaSR<sup>18</sup>. Collectively, these  
502 considerations suggest that the observed phenotype can only be reasonably accounted for by  
503 CaSR ablation from VSMC.

504 ***Features of the phenotype likely to be secondary to disturbed hormone secretion***

505 The hypercalcemia of the  $SM22aCaSR^{\Delta flox/\Delta flox}$  mouse is most likely downstream to the increase  
506 in PTH and particularly 1,25-D<sub>3</sub> levels whereas the observed hypercalciuria is likely secondary  
507 to the hypercalcemia.  $SM22aCaSR^{\Delta flox/\Delta flox}$  mice also showed hyperphosphaturia and  
508 hypophosphatemia, likely *via* FGF23 and PTH induced down-regulation of NaPi2a and thus  
509 decreased phosphate reabsorption from the urine. The mildly increased PTH levels are also

510 plausibly the cause for reduced bone mineral density together with an increase in the bone  
511 resorption in the  $SM22aCaSR^{\Delta flox/\Delta flox}$  mice.

512 The underlying regulatory schemes become more complex when looking at the hormones  
513 themselves. The increase in 1,25-D<sub>3</sub> production could be secondary to the increase in PTH,  
514 though the hyperparathyroidism seems quite mild for such an effect. Also, given that the higher  
515 serum Pi would be expected to limit CaSR activation<sup>47</sup> by extracellular Ca<sup>2+</sup>, the hypercalcemia  
516 and hypophosphatemia seen in the  $SM22aCaSR^{\Delta flox/\Delta flox}$  mice would provide optimal conditions  
517 for enhanced CaSR activation in the parathyroid and thus reduced PTH secretion, instead of  
518 hyperparathyroidism. These observations along with the unaltered Ca<sup>2+</sup>-set point of PTH  
519 secretion from KO PTGs suggest that loss of CaSR in VSMC influences other mechanisms to  
520 promote PTH release *in vivo*.

521 The increase in 1,25-D<sub>3</sub> and PTH could then contribute to the elevated circulating FGF23 levels  
522 which are, at least in part, of skeletal origin given that FGF23 mRNA was undetectable in the  
523 aorta but was increased in the bones of  $SM22aCaSR^{\Delta flox/\Delta flox}$  mice.

#### 524 ***Features of the phenotype likely to be caused by end-organ resistance***

525 1,25-D<sub>3</sub> is a potent inducer of FGF23<sup>48</sup> and, conversely, FGF23 reduces the production of 1,25-  
526 D<sub>3</sub> by downregulating 1 $\alpha$ -hydroxylase<sup>49, 50</sup> and by upregulating 24-hydroxylase<sup>49</sup>. However, in  
527 the  $SM22aCaSR^{\Delta flox/\Delta flox}$  mice, PTH and 1,25-D<sub>3</sub> levels were increased in KO mice despite the  
528 elevated FGF23 levels, indicating resistance of PTH and 1,25-D<sub>3</sub> synthesis to control by FGF23  
529 and pointing away from FGF23 as sole primary factor. It is possible though that the high 1,25-  
530 D<sub>3</sub> and FGF23 levels actually mitigate PTH secretion, contributing to the only relatively mild  
531 increase in serum PTH in these mice – although there seems to be a degree of resistance to 1,25-  
532 D<sub>3</sub> and serum Ca<sup>2+</sup> there as well. Taken together, given its resistance to control by FGF23, 1,25-  
533 D<sub>3</sub> could be the integrating element leading to the combined and complex phenotype observed  
534 in these mice.



535 However, FGF23 resistance does not seem to be a *general* feature of the *SM22a**CaSR* <sup>$\Delta$ flx/ $\Delta$ flx</sup>  
536 mice, as regulation of renal phosphate reabsorption is apparently not affected. A factor that  
537 might play a role here is  $\alpha$ -Klotho, which is acting both locally as co-factor for FGF23 and  
538 systemically in hormonal fashion<sup>51</sup>. Indeed, the observed hypercalcemia, elevated 1,25-D<sub>3</sub> and  
539 FGF23 levels and osteopenia of the *SM22a**CaSR* <sup>$\Delta$ flx/ $\Delta$ flx</sup> mice are, except for the elevated PTH  
540 levels, somewhat reminiscent of the phenotype of the global *Klotho*<sup>-/-</sup> mice (**Table 4**). This  
541 suggests a common role for the VSMC-CaSR and  $\alpha$ -Klotho in Ca<sup>2+</sup> and Pi homeostasis, as  
542 already suggested by the biochemical interaction between CaSR and  $\alpha$ -Klotho in the PTG<sup>52</sup> and  
543 in the kidney<sup>53</sup>. The kidney is the major site of  $\alpha$ -Klotho production<sup>54</sup> where changes in serum  
544 and urinary  $\alpha$ -Klotho mirror those of renal  $\alpha$ -Klotho levels<sup>55</sup>. Interestingly, in the  
545 *SM22a**CaSR* <sup>$\Delta$ flx/ $\Delta$ flx</sup> mice, even though renal  $\alpha$ -Klotho levels were increased, vascular or  
546 circulating  $\alpha$ -Klotho levels were not affected, suggesting that absence of CaSR from VSMC  
547 influences circulating and local  $\alpha$ -Klotho metabolism differently.  
548 Elevated serum FGF23 may be an independent predictor of cardiovascular mortality<sup>56</sup>.  
549 Experimentally, FGF23 alone can directly induce LVH<sup>57</sup> and FGF23 gain of function leads to  
550 volume expansion, hypertension, and cardiac hypertrophy<sup>58</sup>. Despite chronically elevated  
551 FGF23 levels, our *SM22a**CaSR* <sup>$\Delta$ flx/ $\Delta$ flx</sup> mice did not develop LVH at 14 months of age and we  
552 did not observe increased mortality<sup>17, 37</sup>. Since these mice are hypotensive despite their  
553 chronically elevated FGF23 levels, vascular contractility may play a larger role here than  
554 FGF23 mediated renal and cardiac effects on blood pressure.

### 555 ***Renal phenotype***

556 The expression of TRPV5, calbindin D28K and PMCA were all increased in the kidneys of the  
557 *SM22a**CaSR* <sup>$\Delta$ flx/ $\Delta$ flx</sup> mice, suggesting higher transcellular Ca<sup>2+</sup> reabsorption. This increase, due  
558 to chronic elevation of 1,25-D<sub>3</sub>, PTH, and FGF23<sup>58</sup> levels, may contribute to their  
559 hypercalcemia, whereas the increased renal NCC expression is likely to contribute to the

560 observed hypercalciuria, as serum and urine  $Mg^{2+}$  levels were unaffected in KO mice,  
561 suggesting that the abnormality indeed lies within the NCC-expressing distal convoluted  
562 tubule<sup>59</sup>, rather than the thick ascending limb, where  $Ca^{2+}$  and  $Mg^{2+}$  reabsorption happen in  
563 parallel driven by the transepithelial potential difference<sup>60</sup>.

564 The hypercalciuria and hyperphosphaturia of the *SM22a**CaSR* <sup>$\Delta$ lox/ $\Delta$ lox</sup> mice could be the cause for  
565 the formation of the observed micro crystals in their urine. We did not observe nephrolithiasis  
566 in these animals, which can be explained by a CaSR-mediated compensatory mechanism of  
567 urine dilution and acidification. In the collecting duct principal cells, the CaSR<sup>61</sup> is co-expressed  
568 luminally with AQP2<sup>39, 62-65</sup>, and decreases water reabsorption by reducing the apical insertion  
569 of AQP2 water channels. In intercalated cells, the CaSR induces luminal acidification by  
570 activating the V-type H<sup>+</sup> ATPase. In *SM22a**CaSR* <sup>$\Delta$ lox/ $\Delta$ lox</sup> mice, renal AQP2 expression levels  
571 were reduced while urinary excretion of degraded AQP2 was increased, indicating decreased  
572 water reabsorption, and explaining the reduction of urine osmolality. Furthermore, renal V-  
573 ATPase expression was increased in *SM22a**CaSR* <sup>$\Delta$ lox/ $\Delta$ lox</sup> mice compared to WT controls,  
574 explaining their acidified urine.

## 575 **Implications and conclusions**

576 Our study may also have important clinical implications. Physiological pulsation is necessary  
577 for the maintenance of CaSR expression in human aortic smooth muscle cells and may protect  
578 arteries from developing VC<sup>66</sup>. Thus, in early CKD, an increase in arterial stiffness and blood  
579 pressure, could potentially yield a reduction in CaSR expression by VSMC. While absence of  
580 the CaSR apparently does not prompt immediate VC in the blood vessels *in vivo*, it could  
581 contribute to the disease onset *via* the deleterious effects of VSMC-CaSR loss on mineral ion  
582 homeostasis, as observed in our mouse model. A reduction in blood pressure could thus slow  
583 the VSMC-CaSR loss-induced disease progression. Furthermore, a reduction in blood pressure  
584 below what is recommended by most guidelines led to improved cardiovascular and all-cause

585 mortality in the CKD population<sup>67</sup>. Our study supports these findings and points to an early  
586 targeting of blood pressure control to delay CKD progression. Owing to their ability to affect  
587 the VSMC-CaSR, calcimimetics would also be expected to be directly vasculoprotective, in  
588 addition to their systemic effects mediated by suppression of circulating PTH and FGF23 levels.  
589

590 The VSMC-CaSR apparently contributes to mineral ion homeostasis control, possibly by direct  
591 control of FGF23 and 1,25-D<sub>3</sub> production / secretion, though the phenotype of the  
592 *SM22a*CaSR<sup>Δflox/Δflox</sup> mouse is likely to be the result of a combination of disturbances acting  
593 together. Global deletion of the CaSR from VSMC might affect calcium-sensing in all  
594 calcitropic organs to some degree, suggesting a role for the VSMC-CaSR in contributing to  
595 each individual organ's response to mineral ion homeostasis. Further work will be necessary to  
596 dissect the organ-specific paracrine/autocrine responses *vs* whole body endocrine feedback  
597 mechanisms for the fine control of mineral ion homeostasis that the VSMC-CaSR evidently  
598 supports.

599

600 **Author contributions**

601  
602 DR, WC, and MSch designed the study;  
603 MSch, MR, ILF, TSW, SCB, PLY, JG, TM, MSa, CLT, CM, HQ, SAP, DTW, TG, VVM, RAF, AH, JH, CSM and  
604 WC carried out experiments;  
605 MSch, MR, TSW, CM, RAF, UKH, DTW, VVM, TG, CSM, JH, WC, EK and GV analyzed the data;  
606 MSch, MR, TSW and WC made the figures;  
607 MSch, MR, WC, SCB, GV, SAP, VVM, RAF, EK and DR drafted and revised the paper;  
608 All authors approved the final version of the manuscript.

609 **Acknowledgements**

610 The authors want to acknowledge B. Monk, B. van der Kolk, A. Wheatley, P. Edwards, and N.  
611 Kupper for their help with some of the initial experiments and revisions, and Professor AE  
612 Canfield and Dr B. Richards for helpful discussions.

613 **Disclosures**

614 The authors have no disclosures and no competing financial interests.

615 **Funding**

616 EU Marie Curie Innovative Training Network Grant FP7-264663 “Multifaceted CaSR” (to DR,  
617 SAP and EK), Austrian Science Fund P-29948-B28 (to EK), Austrian Science Fund and  
618 Herzfelder’sche Familienstiftung P-32840-B (to MSch), “Intervento cofinanziato dal Fondo di  
619 Sviluppo e Coesione 2007-2013–APQ Ricerca Regione Puglia, Programma Regionale a  
620 Sostegno della Specializzazione Intelligente e della Sostenibilità Sociale ed Ambientale –  
621 FutureInResearch.” CHV NKZ4 (to MR), Kidney Research UK (Intercalated Scholarship) (to  
622 UKH), NIH R01DK12165601, R01DK122259, and VA-BLR&D I01BX005851 and  
623 1IK6BX004835 (to WC).

624

625 **References**

- 626 1. London GM, Marchais SJ, Guerin AP, Metivier F: Arteriosclerosis, vascular calcifications  
627 and cardiovascular disease in uremia. *Curr Opin Nephrol Hypertens*, 14: 525-531, 2005
- 628 2. Villa-Bellosta R, Millan A, Sorribas V: Role of calcium-phosphate deposition in vascular  
629 smooth muscle cell calcification. *Am J Physiol Cell Physiol*, 300: C210-220, 2011  
630 10.1152/ajpcell.00229.2010
- 631 3. Yamada S, Giachelli CM: Vascular calcification in CKD-MBD: Roles for phosphate, FGF23,  
632 and Klotho. *Bone*, 100: 87-93, 2017 10.1016/j.bone.2016.11.012
- 633 4. Block GA, Klassen PS, Lazarus JM, Ofsthun N, Lowrie EG, Chertow GM: Mineral  
634 metabolism, mortality, and morbidity in maintenance hemodialysis. *J Am Soc Nephrol*,  
635 15: 2208-2218, 2004 10.1097/01.ASN.0000133041.27682.A2
- 636 5. Riccardi D, Valenti G: Localization and function of the renal calcium-sensing receptor. *Nat*  
637 *Rev Nephrol*, 12: 414-425, 2016 10.1038/nrneph.2016.59
- 638 6. Yu L, Tomlinson JE, Alexander ST, Hensley K, Han CY, Dwyer D, et al.: Etelcalcetide, A  
639 Novel Calcimimetic, Prevents Vascular Calcification in A Rat Model of Renal  
640 Insufficiency with Secondary Hyperparathyroidism. *Calcif Tissue Int*, 101: 641-653,  
641 2017 10.1007/s00223-017-0319-7
- 642 7. Moe SM, Seifert MF, Chen NX, Sinderson RM, Chen X, Duan D, et al.: R-568 reduces ectopic  
643 calcification in a rat model of chronic kidney disease-mineral bone disorder (CKD-  
644 MBD). *Nephrol Dial Transplant*, 24: 2371-2377, 2009 10.1093/ndt/gfp078
- 645 8. Parfrey PS, Drueke TB, Block GA, Correa-Rotter R, Floege J, Herzog CA, et al.: The Effects  
646 of Cinacalcet in Older and Younger Patients on Hemodialysis: The Evaluation of  
647 Cinacalcet HCl Therapy to Lower Cardiovascular Events (EVOLVE) Trial. *Clin J Am*  
648 *Soc Nephrol*, 10: 791-799, 2015 10.2215/CJN.07730814
- 649 9. Alam MU, Kirton JP, Wilkinson FL, Towers E, Sinha S, Rouhi M, et al.: Calcification is  
650 associated with loss of functional calcium-sensing receptor in vascular smooth muscle  
651 cells. *Cardiovasc Res*, 81: 260-268, 2009 10.1093/cvr/cvn279
- 652 10. Henaut L, Boudot C, Massy ZA, Lopez-Fernandez I, Dupont S, Mary A, et al.:  
653 Calcimimetics increase CaSR expression and reduce mineralization in vascular smooth  
654 muscle cells: mechanisms of action. *Cardiovasc Res*, 101: 256-265, 2014  
655 10.1093/cvr/cvt249
- 656 11. Ciceri P, Elli F, Brenna I, Volpi E, Brancaccio D, Cozzolino M: The Calcimimetic Calindol  
657 Prevents High Phosphate-Induced Vascular Calcification by Upregulating Matrix GLA  
658 Protein. *Nephron Exp Nephrol*, 122: 75-82, 2013 10.1159/000349935
- 659 12. Ciceri P, Volpi E, Brenna I, Elli F, Borghi E, Brancaccio D, et al.: The combination of  
660 lanthanum chloride and the calcimimetic calindol delays the progression of vascular  
661 smooth muscle cells calcification. *Biochem Biophys Res Commun*, 418: 770-773, 2012  
662 10.1016/j.bbrc.2012.01.097
- 663 13. Koleganova N, Piecha G, Ritz E, Schmitt CP, Gross ML: A calcimimetic (R-568), but not  
664 calcitriol, prevents vascular remodeling in uremia. *Kidney Int*, 75: 60-71, 2009  
665 10.1038/ki.2008.490
- 666 14. Mendoza FJ, Martinez-Moreno J, Almaden Y, Rodriguez-Ortiz ME, Lopez I, Estepa JC, et  
667 al.: Effect of calcium and the calcimimetic AMG 641 on matrix-Gla protein in vascular  
668 smooth muscle cells. *Calcif Tissue Int*, 88: 169-178, 2011 10.1007/s00223-010-9442-4
- 669 15. Molostvov G, James S, Fletcher S, Bennett J, Lehnert H, Bland R, et al.: Extracellular  
670 calcium-sensing receptor is functionally expressed in human artery. *Am J Physiol Renal*  
671 *Physiol*, 293: F946-955, 2007 10.1152/ajprenal.00474.2006
- 672 16. Babinsky VN, Hannan FM, Youhanna SC, Marechal C, Jadoul M, Devuyst O, et al.:  
673 Association studies of calcium-sensing receptor (CaSR) polymorphisms with serum

- 674 concentrations of glucose and phosphate, and vascular calcification in renal transplant  
675 recipients. *PLoS one*, 10: e0119459, 2015 10.1371/journal.pone.0119459
- 676 17. Schepelmann M, Yarova PL, Lopez-Fernandez I, Davies TS, Brennan SC, Edwards PJ, et  
677 al.: The vascular Ca<sup>2+</sup>-sensing receptor regulates blood vessel tone and blood pressure.  
678 *Am J Physiol Cell Physiol*, 310: C193-204, 2016 10.1152/ajpcell.00248.2015
- 679 18. Chang W, Tu C, Chen TH, Bikle D, Shoback D: The extracellular calcium-sensing receptor  
680 (CaSR) is a critical modulator of skeletal development. *Sci Signal*, 1: ra1, 2008  
681 10.1126/scisignal.1159945
- 682 19. Holtwick R, Gotthardt M, Skryabin B, Steinmetz M, Potthast R, Zetsche B, et al.: Smooth  
683 muscle-selective deletion of guanylyl cyclase-A prevents the acute but not chronic  
684 effects of ANP on blood pressure. *Proc Natl Acad Sci U S A*, 99: 7142-7147, 2002  
685 10.1073/pnas.102650499
- 686 20. Yarova PL, Stewart AL, Sathish V, Britt RD, Jr., Thompson MA, AP PL, et al.: Calcium-  
687 sensing receptor antagonists abrogate airway hyperresponsiveness and inflammation in  
688 allergic asthma. *Science translational medicine*, 7: 284ra260, 2015  
689 10.1126/scitranslmed.aaa0282
- 690 21. Sage AP, Lu J, Tintut Y, Demer LL: Hyperphosphatemia-induced nanocrystals upregulate  
691 the expression of bone morphogenetic protein-2 and osteopontin genes in mouse smooth  
692 muscle cells in vitro. *Kidney Int*, 79: 414-422, 2011 10.1038/ki.2010.390
- 693 22. Schneider CA, Rasband WS, Eliceiri KW: NIH Image to ImageJ: 25 years of image  
694 analysis. *Nat Methods*, 9: 671-675, 2012
- 695 23. Schindelin J, Arganda-Carreras I, Frise E, Kaynig V, Longair M, Pietzsch T, et al.: Fiji: an  
696 open-source platform for biological-image analysis. *Nat Methods*, 9: 676-682, 2012  
697 10.1038/nmeth.2019
- 698 24. Sun Y, Yu H, Zheng D, Cao Q, Wang Y, Harris D, et al.: Sudan black B reduces  
699 autofluorescence in murine renal tissue. *Arch Pathol Lab Med*, 135: 1335-1342, 2011  
700 10.5858/arpa.2010-0549-OA
- 701 25. Puchtler H, Meloan SN, Terry MS: On the history and mechanism of alizarin and alizarin  
702 red S stains for calcium. *J Histochem Cytochem*, 17: 110-124, 1969
- 703 26. Jono S, Nishizawa Y, Shioi A, Morii H: Parathyroid hormone-related peptide as a local  
704 regulator of vascular calcification. Its inhibitory action on in vitro calcification by  
705 bovine vascular smooth muscle cells. *Arterioscler Thromb Vasc Biol*, 17: 1135-1142,  
706 1997
- 707 27. Moorehead WR, Biggs HG: 2-Amino-2-methyl-1-propanol as the alkalizing agent in an  
708 improved continuous-flow cresolphthalein complexone procedure for calcium in serum.  
709 *Clin Chem*, 20: 1458-1460, 1974
- 710 28. Leroux-Berger M, Queguiner I, Maciel TT, Ho A, Relaix F, Kempf H: Pathologic  
711 calcification of adult vascular smooth muscle cells differs on their crest or mesodermal  
712 embryonic origin. *J Bone Miner Res*, 26: 1543-1553, 2011 10.1002/jbmr.382
- 713 29. Cheng Z, Liang N, Chen TH, Li A, Santa Maria C, You M, et al.: Sex and age modify  
714 biochemical and skeletal manifestations of chronic hyperparathyroidism by altering  
715 target organ responses to Ca<sup>2+</sup> and parathyroid hormone in mice. *J Bone Miner Res*,  
716 28: 1087-1100, 2013 10.1002/jbmr.1846
- 717 30. Ranieri M, Tamma G, Di Mise A, Russo A, Centrone M, Svelto M, et al.: Negative feedback  
718 from CaSR signaling to aquaporin-2 sensitizes vasopressin to extracellular Ca<sup>2+</sup>. *Journal*  
719 *of cell science*, 128: 2350-2360, 2015 10.1242/jcs.168096
- 720 31. Graca JA, Schepelmann M, Brennan SC, Reens J, Chang W, Yan P, et al.: Comparative  
721 expression of the extracellular calcium-sensing receptor in the mouse, rat, and human  
722 kidney. *Am J Physiol Renal Physiol*, 310: F518-533, 2016 10.1152/ajprenal.00208.2015
- 723 32. Tamma G, Lasorsa D, Ranieri M, Mastrofrancesco L, Valenti G, Svelto M: Integrin  
724 signaling modulates AQP2 trafficking via Arg-Gly-Asp (RGD) motif. *Cellular*

- 725 *physiology and biochemistry : international journal of experimental cellular*  
726 *physiology, biochemistry, and pharmaco*, 27: 739-748, 2011 10.1159/000330082
- 727 33. Trimpert C, van den Berg DT, Fenton RA, Klussmann E, Deen PM: Vasopressin increases  
728 S261 phosphorylation in AQP2-P262L, a mutant in recessive nephrogenic diabetes  
729 insipidus. *Nephrology, dialysis, transplantation : official publication of the European*  
730 *Dialysis and Transplant Associatio*, 27: 4389-4397, 2012 10.1093/ndt/gfs292
- 731 34. Sadler AM, Bailey SJ: Validation of a refined technique for taking repeated blood samples  
732 from juvenile and adult mice. *Lab Anim*, 47: 316-319, 2013  
733 10.1177/0023677213494366
- 734 35. Procino G, Mastrofrancesco L, Tamma G, Lasorsa DR, Ranieri M, Stringini G, et al.:  
735 Calcium-sensing receptor and aquaporin 2 interplay in hypercalciuria-associated renal  
736 concentrating defect in humans. An in vivo and in vitro study. *PLoS one*, 7: e33145,  
737 2012 10.1371/journal.pone.0033145
- 738 36. Tamma G, Di Mise A, Ranieri M, Svelto M, Pisot R, Bilancio G, et al.: A decrease in  
739 aquaporin 2 excretion is associated with bed rest induced high calciuria. *J Transl Med*,  
740 12: 133, 2014 10.1186/1479-5876-12-133
- 741 37. Yarova PL, Stewart AL, Sathish V, Britt RD, Jr., Thompson MA, AP PL, et al.: Calcium-  
742 sensing receptor antagonists abrogate airway hyperresponsiveness and inflammation in  
743 allergic asthma. *Sci Transl Med*, 7: 284ra260, 2015 10.1126/scitranslmed.aaa0282
- 744 38. Alexander RT, Woudenberg-Vrenken TE, Buurman J, Dijkman H, van der Eerden BC, van  
745 Leeuwen JP, et al.: Klotho prevents renal calcium loss. *J Am Soc Nephrol*, 20: 2371-  
746 2379, 2009 10.1681/ASN.2008121273
- 747 39. Ranieri M, Zahedi K, Tamma G, Centrone M, Di Mise A, Soleimani M, et al.: CaSR  
748 signaling down-regulates AQP2 expression via a novel microRNA pathway in pendrin  
749 and NaCl cotransporter knockout mice. *FASEB J*, 32: 2148-2159, 2018  
750 10.1096/fj.201700412RR
- 751 40. London GM, Guerin AP, Marchais SJ, Metivier F, Pannier B, Adda H: Arterial media  
752 calcification in end-stage renal disease: impact on all-cause and cardiovascular  
753 mortality. *Nephrol Dial Transplant*, 18: 1731-1740, 2003 10.1093/ndt/gfg414
- 754 41. Raggi P, Boulay A, Chasan-Taber S, Amin N, Dillon M, Burke SK, et al.: Cardiac  
755 calcification in adult hemodialysis patients. A link between end-stage renal disease and  
756 cardiovascular disease? *J Am Coll Cardiol*, 39: 695-701, 2002 10.1016/s0735-  
757 1097(01)01781-8
- 758 42. Torremade N, Bozic M, Panizo S, Barrio-Vazquez S, Fernandez-Martin JL, Encinas M, et  
759 al.: Vascular Calcification Induced by Chronic Kidney Disease Is Mediated by an  
760 Increase of 1alpha-Hydroxylase Expression in Vascular Smooth Muscle Cells. *J Bone*  
761 *Miner Res*, 31: 1865-1876, 2016 10.1002/jbmr.2852
- 762 43. Adeney KL, Siscovick DS, Ix JH, Seliger SL, Shlipak MG, Jenny NS, et al.: Association of  
763 serum phosphate with vascular and valvular calcification in moderate CKD. *J Am Soc*  
764 *Nephrol*, 20: 381-387, 2009 10.1681/ASN.2008040349
- 765 44. Ho C, Conner DA, Pollak MR, Ladd DJ, Kifor O, Warren HB, et al.: A mouse model of  
766 human familial hypocalciuric hypercalcemia and neonatal severe hyperparathyroidism.  
767 *Nat Genet*, 11: 389-394, 1995 10.1038/ng1295-389
- 768 45. Chang W, Tu CL, Jean-Alphonse FG, Herberger A, Cheng Z, Hwong J, et al.: PTH  
769 hypersecretion triggered by a GABAB1 and Ca(2+)-sensing receptor heterocomplex in  
770 hyperparathyroidism. *Nat Metab*, 2: 243-255, 2020 10.1038/s42255-020-0175-z
- 771 46. Toka HR, Al-Romaih K, Koshy JM, DiBartolo S, 3rd, Kos CH, Quinn SJ, et al.: Deficiency  
772 of the calcium-sensing receptor in the kidney causes parathyroid hormone-independent  
773 hypocalciuria. *J Am Soc Nephrol*, 23: 1879-1890, 2012 10.1681/ASN.2012030323

- 774 47. Centeno PP, Herberger A, Mun HC, Tu C, Nemeth EF, Chang W, et al.: Phosphate acts  
775 directly on the calcium-sensing receptor to stimulate parathyroid hormone secretion.  
776 *Nat Commun*, 10: 4693, 2019 10.1038/s41467-019-12399-9
- 777 48. Saito H, Maeda A, Ohtomo S, Hirata M, Kusano K, Kato S, et al.: Circulating FGF-23 is  
778 regulated by 1alpha,25-dihydroxyvitamin D3 and phosphorus in vivo. *J Biol Chem*,  
779 280: 2543-2549, 2005 10.1074/jbc.M408903200
- 780 49. Shimada T, Hasegawa H, Yamazaki Y, Muto T, Hino R, Takeuchi Y, et al.: FGF-23 is a  
781 potent regulator of vitamin D metabolism and phosphate homeostasis. *J Bone Miner*  
782 *Res*, 19: 429-435, 2004 10.1359/JBMR.0301264
- 783 50. Shimada T, Kakitani M, Yamazaki Y, Hasegawa H, Takeuchi Y, Fujita T, et al.: Targeted  
784 ablation of Fgf23 demonstrates an essential physiological role of FGF23 in phosphate  
785 and vitamin D metabolism. *J Clin Invest*, 113: 561-568, 2004 10.1172/JCI19081
- 786 51. Dalton GD, Xie J, An SW, Huang CL: New Insights into the Mechanism of Action of  
787 Soluble Klotho. *Front Endocrinol (Lausanne)*, 8: 323, 2017 10.3389/fendo.2017.00323
- 788 52. Fan Y, Liu W, Bi R, Densmore MJ, Sato T, Mannstadt M, et al.: Interrelated role of Klotho  
789 and calcium-sensing receptor in parathyroid hormone synthesis and parathyroid  
790 hyperplasia. *Proc Natl Acad Sci U S A*, 115: E3749-E3758, 2018  
791 10.1073/pnas.1717754115
- 792 53. Yoon J, Liu Z, Lee E, Liu L, Ferre S, Pastor J, et al.: Physiologic Regulation of Systemic  
793 Klotho Levels by Renal CaSR Signaling in Response to CaSR Ligands and pHo. *J Am*  
794 *Soc Nephrol*, 2021 10.1681/ASN.2021020276
- 795 54. Kuro-o M, Matsumura Y, Aizawa H, Kawaguchi H, Suga T, Utsugi T, et al.: Mutation of  
796 the mouse klotho gene leads to a syndrome resembling ageing. *Nature*, 390: 45-51, 1997  
797 10.1038/36285
- 798 55. Hu MC, Shi M, Zhang J, Quinones H, Griffith C, Kuro-o M, et al.: Klotho deficiency causes  
799 vascular calcification in chronic kidney disease. *J Am Soc Nephrol*, 22: 124-136, 2011  
800 10.1681/ASN.2009121311
- 801 56. Arnlov J, Carlsson AC, Sundstrom J, Ingelsson E, Larsson A, Lind L, et al.: Serum FGF23  
802 and risk of cardiovascular events in relation to mineral metabolism and cardiovascular  
803 pathology. *Clin J Am Soc Nephrol*, 8: 781-786, 2013 10.2215/CJN.09570912
- 804 57. Faul C, Amaral AP, Oskoueï B, Hu MC, Sloan A, Isakova T, et al.: FGF23 induces left  
805 ventricular hypertrophy. *J Clin Invest*, 121: 4393-4408, 2011 10.1172/JCI46122
- 806 58. Andrukhova O, Slavic S, Smorodchenko A, Zeitz U, Shalhoub V, Lanske B, et al.: FGF23  
807 regulates renal sodium handling and blood pressure. *EMBO Mol Med*, 6: 744-759, 2014  
808 10.1002/emmm.201303716
- 809 59. Subramanya AR, Ellison DH: Distal convoluted tubule. *Clin J Am Soc Nephrol*, 9: 2147-  
810 2163, 2014 10.2215/CJN.05920613
- 811 60. de Rouffignac C, Quamme G: Renal magnesium handling and its hormonal control. *Physiol*  
812 *Rev*, 74: 305-322, 1994 10.1152/physrev.1994.74.2.305
- 813 61. Renkema KY, Velic A, Dijkman HB, Verkaart S, van der Kemp AW, Nowik M, et al.: The  
814 calcium-sensing receptor promotes urinary acidification to prevent nephrolithiasis. *J Am*  
815 *Soc Nephrol*, 20: 1705-1713, 2009 10.1681/ASN.2008111195
- 816 62. Ranieri M: Renal Ca(2+) and Water Handling in Response to Calcium Sensing Receptor  
817 Signaling: Physiopathological Aspects and Role of CaSR-Regulated microRNAs. *Int J*  
818 *Mol Sci*, 20, 2019 10.3390/ijms20215341
- 819 63. Sands JM, Naruse M, Baum M, Jo I, Hebert SC, Brown EM, et al.: Apical extracellular  
820 calcium/polyvalent cation-sensing receptor regulates vasopressin-elicited water  
821 permeability in rat kidney inner medullary collecting duct. *J Clin Invest*, 99: 1399-1405,  
822 1997 10.1172/JCI119299



- 823 64. Riccardi D, Brown EM: Physiology and pathophysiology of the calcium-sensing receptor  
824 in the kidney. *Am J Physiol Renal Physiol*, 298: F485-499, 2010  
825 10.1152/ajprenal.00608.2009
- 826 65. Brown EM: Physiology and pathophysiology of the extracellular calcium-sensing receptor.  
827 *Am J Med*, 106: 238-253, 1999
- 828 66. Molostvov G, Hiemstra TF, Fletcher S, Bland R, Zehnder D: Arterial Expression of the  
829 Calcium-Sensing Receptor Is Maintained by Physiological Pulsation and Protects  
830 against Calcification. *PLoS one*, 10: e0138833, 2015 10.1371/journal.pone.0138833
- 831 67. Gosmanova EO, Kovesdy CP: Blood Pressure Targets in CKD: Lessons Learned from  
832 SPRINT and Previous Observational Studies. *Curr Cardiol Rep*, 18: 88, 2016  
833 10.1007/s11886-016-0769-y
- 834 68. Kaludjerovic J, Komaba H, Lanske B: Effects of klotho deletion from bone during chronic  
835 kidney disease. *Bone*, 100: 50-55, 2017 10.1016/j.bone.2017.02.006  
836

837

838 **Supplemental Material Table of Contents**

839

840 Page numbers refer to the *supplemental material\_revised.pdf*

Table S1 Pg. 2

Table S2 Pg. 3

Figure S1 Pg. 4

Figure S2 Pg. 5

Figure S3 Pg. 6

Figure S4 Pg. 7

Figure S5 Pg. 8

Figure S6 Pg. 9

Figure S7 Pg. 10

Figure S8 Pg. 11

841

842

843 **Tables**

844 **Table 1: Blood biochemistry of 3-month-old WT and KO mice.** 1,25-D<sub>3</sub> = 1,25-dihydroxy  
 845 vitamin D / calcitriol, BUN = blood urea nitrogen. \*  $p < 0.05$ , \*\*  $p < 0.01$ , \*\*\*  $p < 0.001$ , mean  
 846  $\pm$  SD, two-tailed T-test.

Parameter	Unit	WT	N	KO	N	<i>p</i> -value
Na <sup>+</sup>	mmol / l	145.35 $\pm$ 2.77	17	144.15 $\pm$ 3.84	10	0.3540
Cl <sup>-</sup>	mmol / l	109.18 $\pm$ 3.34	17	108.45 $\pm$ 4.82	10	0.6472
K <sup>+</sup>	mmol / l	5.24 $\pm$ 0.40	3	5.62 $\pm$ 0.18	3	0.2092
Ca <sup>2+</sup>	mmol / l	2.28 $\pm$ 0.21	28	2.94 $\pm$ 0.59	21	<0.0001 ***
Mg <sup>2+</sup>	mmol / l	1.06 $\pm$ 0.12	22	1.15 $\pm$ 0.22	20	0.0979
FGF23	pg / ml	145.0 $\pm$ 36.4	11	384.4 $\pm$ 204.5	6	0.0015 **
Pi	mmol / l	2.36 $\pm$ 0.45	17	1.94 $\pm$ 0.47	16	0.0146 *
Hematocrit	%	40.3 $\pm$ 7.6	9	38.9 $\pm$ 8.6	6	0.7407
PTH	pg / ml	151.7 $\pm$ 115.5	30	256.6 $\pm$ 249.8	30	0.0411 *
1,25-D <sub>3</sub>	pmol / l	162.1 $\pm$ 81.3	19	310.8 $\pm$ 173.4	17	0.0020 **
$\alpha$ -Klotho	pg / ml	555.4 $\pm$ 164.6	13	564.7 $\pm$ 389.3	11	0.9379
Aldosterone	pg / ml	508.1 $\pm$ 199.0	12	421.8 $\pm$ 205.2	12	0.3072
Renin	pg / ml	123.8 $\pm$ 58.0	12	115.4 $\pm$ 40.3	12	0.6850
Fetuin A	$\mu$ g / ml	201.4 $\pm$ 40.9	12	193.0 $\pm$ 40.8	12	0.6175
PPi	$\mu$ mol / l	34.1 $\pm$ 40.8	12	25.0 $\pm$ 14.2	12	0.4747
Albumin	mg / ml	29.4 $\pm$ 1.4	11	27.6 $\pm$ 1.7	11	0.0179 *
ALP	U / l	81.73 $\pm$ 11.38	11	100.18 $\pm$ 22.74	11	0.0297 *
Creatinine	$\mu$ mol / l	15.4 $\pm$ 1.6	6	13.0 $\pm$ 1.3	5	0.0265 *
Urea	mmol / l	10.1 $\pm$ 1.3	6	10.4 $\pm$ 0.3	5	0.6474
BUN	mmol / l	8.4 $\pm$ 2.4	11	8.7 $\pm$ 1.8	11	0.7781
Total Protein	mg / ml	54.4 $\pm$ 3.0	6	51.2 $\pm$ 2.6	4	0.1196

847

848

849 **Table 2: Urine chemistry of 3-month-old WT and KO mice.** Averages of measurements  
850 from two consecutive 24 h urine collections. Cr = creatinine, d = 24 h, BW = body weight (g),  
851 Na<sup>+</sup>, Cl<sup>-</sup>, K<sup>+</sup>, Ca<sup>2+</sup>, Mg<sup>2+</sup>, and Pi are normalised to individual creatinine levels of each mouse.  
852 Creatinine, total urinary protein, urea, uric acid, and glucose are normalised to 24 h urine  
853 production per bodyweight of each mouse. \* *p* < 0.05, \*\*\* *p* < 0.001, mean ± SD, two-tailed  
854 T-test.

Parameter	Unit	WT	N	KO	N	<i>p</i> -value
Na <sup>+</sup> :Cr	mmol / mmol	37.32 ± 9.93	6	34.06 ± 12.57	6	0.6290
Cl <sup>-</sup> :Cr	mmol / mmol	70.18 ± 10.93	6	69.25 ± 19.70	6	0.9215
K <sup>+</sup> :Cr	mmol / mmol	50.25 ± 9.27	6	58.62 ± 8.86	6	0.1410
Ca <sup>2+</sup> :Cr	mmol / mmol	0.90 ± 0.55	6	6.48 ± 4.56	6	0.0140 *
Mg <sup>2+</sup> :Cr	mmol / mmol	6.40 ± 1.81	4	8.05 ± 3.19	3	0.4184
Pi:Cr	mmol / mmol	7.84 ± 2.98	6	22.45 ± 5.92	6	0.0003 ***
Cr	μmol / (d * BW)	0.230 ± 0.038	6	0.221 ± 0.061	6	0.7548
Total protein	μg / (d * BW)	197.43 ± 112.49	6	176.34 ± 104.42	6	0.7435
Urea	μmol / (d * BW)	80.23 ± 21.42	6	80.42 ± 19.88	6	0.9876
Uric acid	μmol / (d * BW)	37.33 ± 8.20	6	32.30 ± 11.60	6	0.4069
Glucose	μmol / (d * BW)	0.133 ± 0.030	6	0.219 ± 0.178	6	0.2694
24h urine	mg / h / BW	2.50 ± 0.56	6	2.98 ± 0.60	5	0.1999

855

856

857

858 **Table 3: Results of  $\mu$ CT analysis of hind-leg bones from 3-month-old WT and KO mice.**

859 Bone parameter abbreviations: Tb = trabecular bone at the distal femur, Ct = cortical bone at  
 860 the tibio-fibular junction, TV = total volume, BV = bone volume, BV/TV = bone volume  
 861 fraction, CD = connectivity density, SMI = structure model index, N = trabecular number, Th  
 862 = thickness, Sp = spacing, BMD = bone mineral density. AU = arbitrary units. Mean  $\pm$  SD, \*  $p$   
 863 < 0.05, \*\*  $p$  < 0.01, two-tailed Student's t-test.

Parameter	Unit	WT	N	KO	N	$p$ -value
Tb.TV	mm <sup>3</sup>	2.13 $\pm$ 0.25	8	1.88 $\pm$ 0.15	9	0.0238 *
Tb.BV	mm <sup>3</sup>	0.33 $\pm$ 0,05	8	0.24 $\pm$ 0.04	9	0.0014 **
Tb.BV/TV	ratio	0.16 $\pm$ 0.02	8	0.13 $\pm$ 0.02	9	0.0133 *
Tb.CD	1/mm <sup>3</sup>	369.62 $\pm$ 39.79	8	285.25 $\pm$ 49.53	9	0.0016 **
Tb.SMI	AU	2.07 $\pm$ 0.28	8	2.37 $\pm$ 0.15	9	0.0123 *
Tb.N	1/mm <sup>3</sup>	5.91 $\pm$ 0.42	8	5.08 $\pm$ 0.80	9	0.0189 *
Tb.Th	$\mu$ m	39.09 $\pm$ 5.94	8	37.30 $\pm$ 4.49	9	0.4915
Tb.Sp	mm	0.17 $\pm$ 0.01	8	0.19 $\pm$ 0.02	9	0.0140 *
Tb.BMD	AU	1164.85 $\pm$ 8.75	8	1138.54 $\pm$ 23.69	9	0.0098 **
Ct.TV	mm <sup>3</sup>	0.40 $\pm$ 0.03	8	0.39 $\pm$ 0.04	9	0.3678
Ct.BV	mm <sup>3</sup>	0.27 $\pm$ 0.02	8	0.25 $\pm$ 0.03	9	0.1977
Ct.BV/TV	ratio	0.66 $\pm$ 0.03	8	0.66 $\pm$ 0.03	9	0.5431
Ct.BMD	AU	1433.39 $\pm$ 33.25	8	1394.06 $\pm$ 16.96	9	0.0069 **
Ct.Th	$\mu$ m	235.13 $\pm$ 15.15	8	226.56 $\pm$ 13.38	9	0.2344

864

865

866

867 **Table 4: Comparison of the *Klotho*<sup>-/-</sup>, *PTG-CaSR*<sup>-/-</sup>, *Renal-CaSR*<sup>-/-</sup> and *VSMC-CaSR*<sup>-/-</sup>**  
 868 **mice.** Arrows: (fold changes compared to control animals) =: no change, 1-2: ↓/↑; 2-3: ↓↓/↑↑;  
 869 >3: ↓↓↓/↑↑↑, n.d.: not determined

Parameter	<i>Klotho</i> deficient <sup>54, 68</sup>	<i>PTG-CaSR</i> <sup>-/- 18</sup>	<i>Renal-CaSR</i> <sup>-/- 46</sup>	<i>VSMC-CaSR</i> <sup>-/-</sup>
Plasma Ca <sup>2+</sup>	↑	↑↑	=	↑
Urinary Ca <sup>2+</sup>	n.d.	↑↑↑	↓↓↓	↑↑↑
Plasma Pi	↑	n.d.	=	↓
Urinary Pi	↑	n.d.	n.d.	↑↑
Plasma 1,25-D <sub>3</sub>	↑↑	n.d.	=	↑↑
Plasma PTH	↓	↑↑↑	=	↑
FGF23	↑↑	n.d.	n.d.	↑↑
Body weight	↓↓	↓↓↓	=	=/↓
BMD	↓	↓↓↓	=	↓

870

871 **Figure legends**

872 **Figure 1: *In vitro* calcification of isolated VSMC. A:** Photograph of 24-well microplates with  
873 cultured VSMC from WT (left two plates) and KO mouse aortas (right two plates) incubated  
874 for 10 days with a series of  $\text{Ca}^{2+}$  (numbers: mM  $\text{Ca}^{2+}$  in the 3 horizontally adjacent wells) /  
875 phosphate (Pi) concentrations (top two plates: 2 mM Pi, bottom two plates: 3 mM Pi) in the  
876 growth medium. Cells were then fixed and stained with Alizarin Red S. Darker spots indicate  
877 calcium deposits. At 2 mM Pi, WT did not show any calcification independent of the  $\text{Ca}^{2+}$   
878 concentration, while VSMC from KO mice started to show calcification at 1.6 mM  $\text{Ca}^{2+}$ . At 3  
879 mM Pi, WT cells started to calcify at 1.6 mM  $\text{Ca}^{2+}$  and KO cells at 1.2 mM  $\text{Ca}^{2+}$ . **B:**  
880 Quantification of  $\text{Ca}^{2+}$  deposition in WT and KO cells at 3 mM Pi and 1.2, 1.8 or 2.5 mM  $\text{Ca}^{2+}$   
881 using o-cresolphthalein complexone assay, normalised to the amount of protein (BCA assay)  
882 and the normocalcemic (1.2 mM  $\text{Ca}^{2+}$ ) control. Friedmann with Dunn post-hoc test. **C:**  
883 Quantification of  $\text{Ca}^{2+}$  deposition in WT and KO cells at 3 mM Pi and 1.2 mM  $\text{Ca}^{2+}$  in the  
884 presence or absence of 10 nM calcimimetic R-568. Median $\pm$ IQR, Mann-Whitney-U test. \*  $p <$   
885 0.05, \*\*  $p <$  0.01.

886

887 **Figure 2: Aorta mRNA expression levels and quantitative immunohistochemistry. A:**  
888 *Klotho*, **B:** *Cyp27b1*, and **C:** *Sm22 $\alpha$*  mRNA expression levels relative to calibrator (mean  $\Delta\text{CT}$   
889 WT). **D & E:** quantitative immunohistochemistry analysis of  $\alpha$ -Klotho in smooth muscle and  
890 endothelial layer of WT and KO aorta sections. Mean grey values (lower = darker). **F:**  
891 representative stainings for  $\alpha$ -Klotho used for quantification. **G & H:** quantitative  
892 immunohistochemistry analysis of CYP27B1 in smooth muscle and endothelial layer of WT  
893 and KO aorta sections. Mean grey values (lower = darker). **I:** representative stainings for  
894 CYP27B1 used for quantification. Inserts = IgG negative control. Inserts = IgG negative  
895 control. Scale bars = 50  $\mu\text{m}$ .

896

897 **Figure 3: Kidney calcium handling and CaSR expression in  $SM22\alpha$ CaSR $\Delta$ flox/ $\Delta$ flox mice. A-B:**

898 semi-quantitative Western blot analyses of  $\square$ -Klotho and the sodium phosphate cotransporter,

899 NaPi2a. C-F: quantitative immunohistochemistry of the vitamin D receptor (VDR), the calcium

900 channel Transient Receptor Potential cation channel subfamily V member 5 (TRPV5),

901 calbindin (D28K) and the plasma membrane calcium ATPase (PMCA). G: CaSR mRNA

902 expression in whole kidney lysate relative to calibrator (mean  $\Delta$ CT of WT). H: quantitative

903 immunofluorescence analysis of CaSR expression in kidney sections. I: semi-quantitative

904 Western blot analysis of CaSR protein expression in whole kidney lysates. Mean $\pm$ SD, \*  $p <$

905 0.05, \*\*  $p < 0.01$ , \*\*\*  $p < 0.001$ , two-tailed Student's t-test.

906

907 **Figure 4: Kidney water transport in  $SM22\alpha$ CaSR $\Delta$ flox/ $\Delta$ flox mice. A:** Optical microscopy images

908 of crystal precipitates in urines from WT and KO mice (scale bar: 100  $\mu$ m). B: Urine osmolality

909 and C: urine pH of WT and KO mice from two consecutive days in metabolic cages. Mean $\pm$ SD,

910 \*\*  $p < 0.01$ , \*\*\*  $p < 0.001$  for overall genotype effect, two-way ANOVA. D-H: semi-

911 quantitative Western blot analyses of the thiazide sensitive sodium-chloride cotransporter

912 (NCC), V-H<sup>+</sup>-ATPase, total aquaporin 2 (AQP2), pS261-AQP2, pS256-AQP2 in WT and KO

913 kidney lysates. I: AQP2 excretion measured by ELISA assay in urines from WT and KO.

914 Mean $\pm$ SD, \*  $p < 0.05$ , \*\*  $p < 0.01$ , two-tailed Student's t-test.

915

916 **Figure 5: Analysis of the parathyroid glands. A:** Micrographs of isolated parathyroid glands

917 from WT and KO mice. Scale bar = 500  $\mu$ m. B: Immunofluorescence images of isolated

918 parathyroid glands from WT and KO mice, showing comparable staining intensity for the

919 CaSR. Scale bar = 50  $\mu$ m. C: Western Blot analysis of CaSR expression in parathyroid glands,

920 showing equal expression of both the monomer (~130 kDa) and the dimer (~250 kDa) of the

921 CaSR. D: PTH release assay in response to increases in extracellular Ca<sup>2+</sup>. Left panel: raw data,



922 right panel: normalised to PTH release at 0.5 mM  $\text{Ca}^{2+}$  = 100 % for both WT and KO. Vertical  
923 lines indicate  $\text{Ca}^{2+}$  concentration at half maximal PTH response. N = 3, < 1.4 % total variance  
924 explained by genotype as determined by repeated measures two-way ANOVA.

925

926 **Figure 6: Phenotype of the *SM22 $\alpha$* CaSR <sup>$\Delta$ flox/ $\Delta$ flox</sup> mice.** Continuous lines = stimulation, broken  
927 lines = inhibition. Greyed out lines = loss of action due to VSMC-CaSR deletion.

928 Loss of the CaSR in VSMC affects whole body mineral ion homeostasis leading to the loss  
929 (red X signs) of an inhibitory function on the production / secretion of 1,25-D<sub>3</sub>, PTH, and  
930 FGF23. At the same time, VSMC-CaSR loss apparently also affects or overrides hormonal  
931 control: 1,25-D<sub>3</sub> synthesis is apparently resistant to control by FGF23, while PTH secretion is  
932 (slightly) increased, pointing to some degree of resistance to control by 1,25-D<sub>3</sub>, FGF23, and  
933 serum calcium (despite a fully functional CaSR in the parathyroid glands). The increased  
934 1,25-D<sub>3</sub> and PTH leads to hypercalcemia followed by hypercalciuria. Pi excretion is increased  
935 as a result of the increased PTH and FGF23 levels, leading to low serum Pi. Urine osmolality  
936 and pH are decreased to prevent nephrolithiasis. The urinary calcium and phosphate wasting  
937 then contributes to the observed bone loss in these animals (not shown in the scheme). Owing  
938 to the presence of blood vessels in all organs of the body, it remains to be elucidated whether  
939 all the observed features of this phenotype are primary to CaSR deletion from the VSMC,  
940 secondary compensatory mechanisms, or a combination of both.

Figure 1

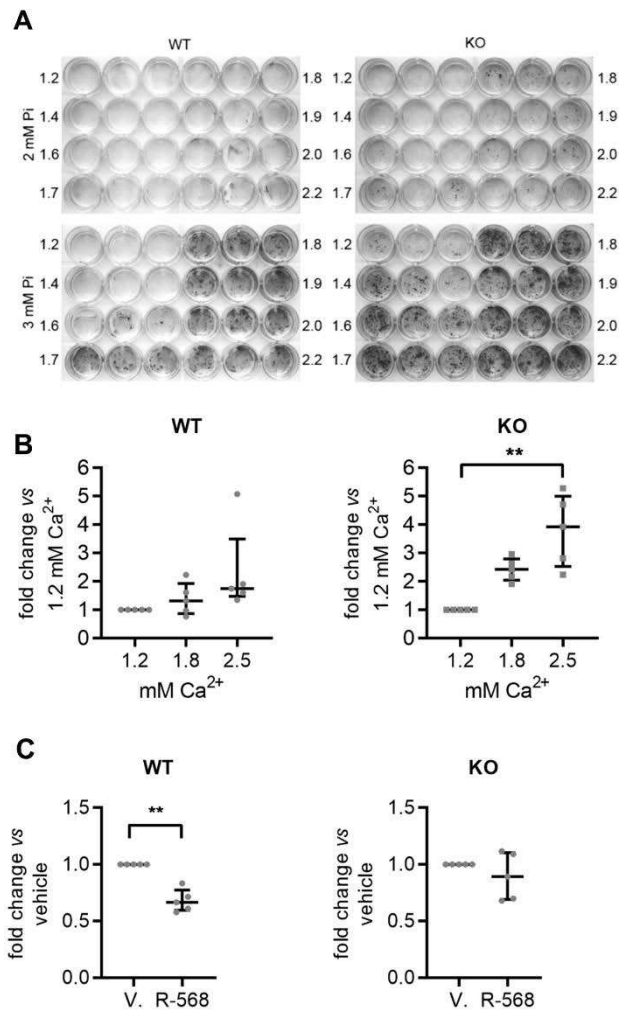


Figure 2

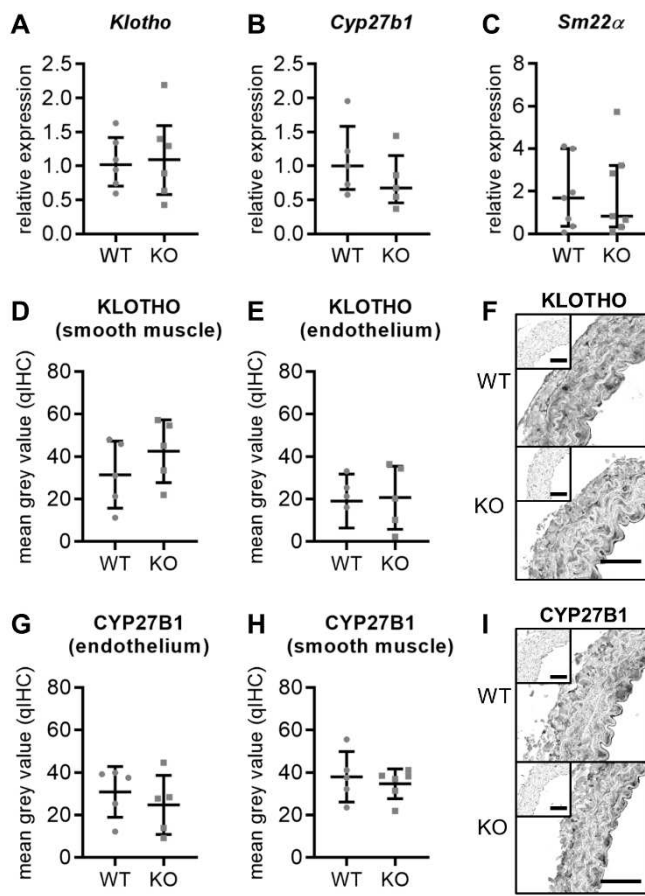


Figure 3

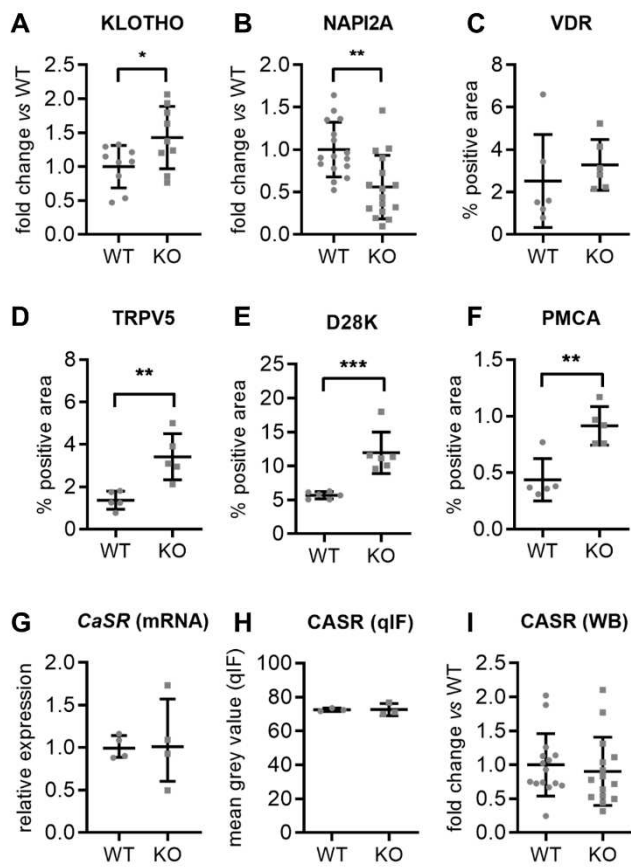


Figure 4

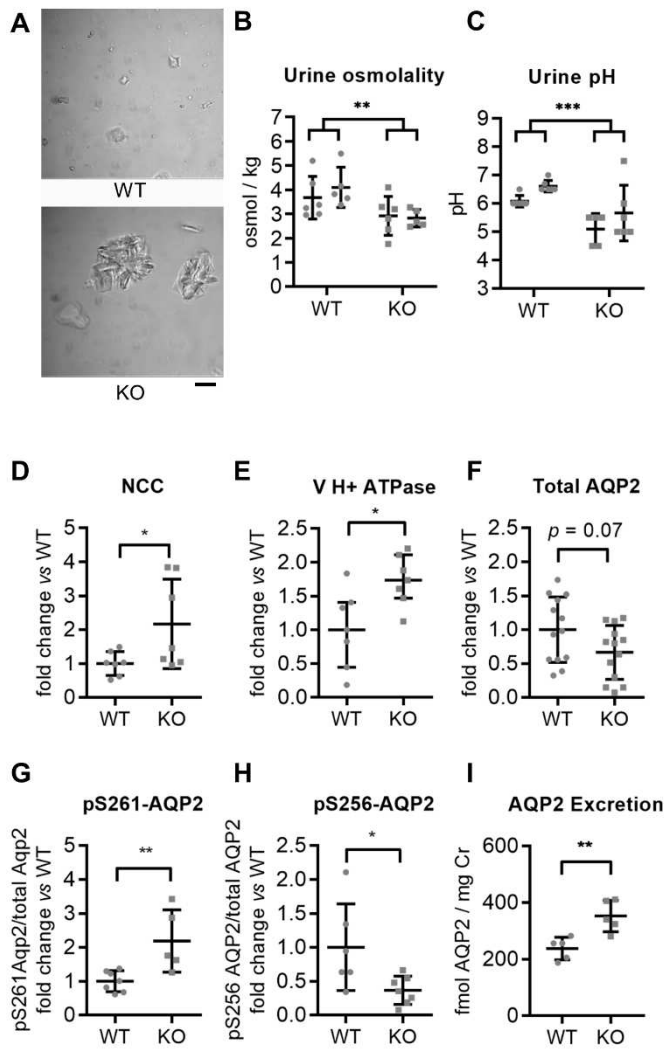


Figure 5

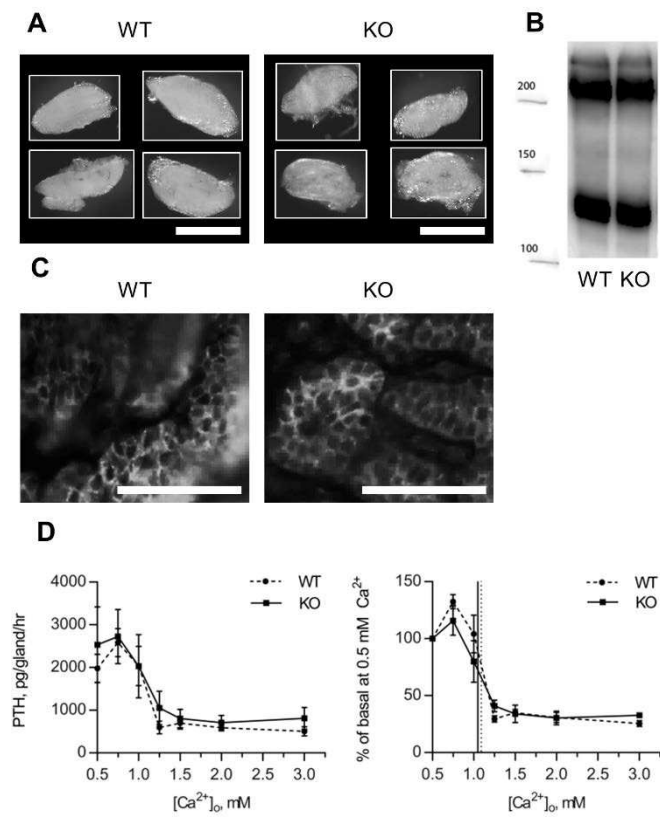
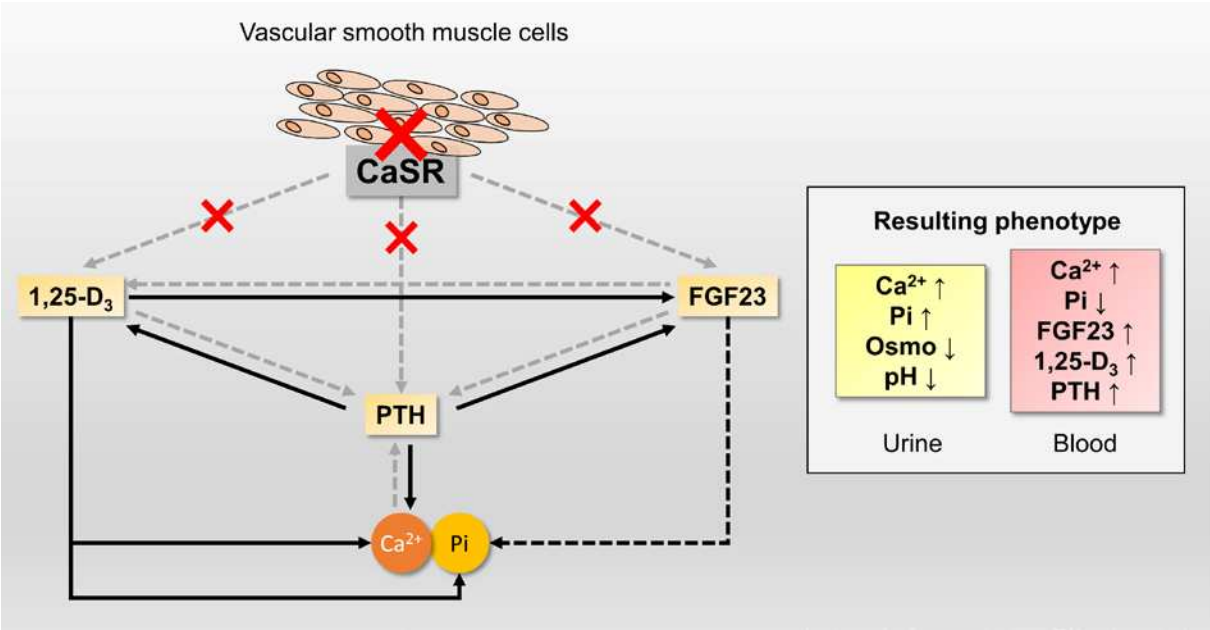


Figure 6



# Supplemental material

## Table of contents

Table S1	Pg. 2
Table S2	Pg. 3
Figure S1	Pg. 4
Figure S2	Pg. 5
Figure S3	Pg. 6
Figure S4	Pg. 7
Figure S5	Pg. 8
Figure S6	Pg. 9
Figure S7	Pg. 10
Figure S8	Pg. 11



**Table S1: Blood biochemistry of 18-month-old WT and KO mouse.** \*  $p < 0.05$ , \*\*  $p < 0.01$ , mean  $\pm$  SD, two-tailed T-test. “CaSR” indicates concentration of N-terminal soluble CaSR / CaSR-fragment. Osmolality and CaSR were measured in male and female mice.

Parameter	Unit	WT	N	KO	N	<i>p</i> -value
Na <sup>+</sup>	mmol / l	149.0 $\pm$ 3.61	3	146.3 $\pm$ 3.06	3	0.3837
K <sup>+</sup>	mmol/l	10.64 $\pm$ 0.61	3	11.88 $\pm$ 2.53	3	0.4541
Cl <sup>-</sup>	mmol / l	114.33 $\pm$ 1.15	3	111.00 $\pm$ 3.61	3	0.2020
Ca <sup>2+</sup>	mmol / l	2.34 $\pm$ 0.13	3	2.99 $\pm$ 0.35	3	0.0401 *
Mg <sup>2+</sup>	mmol / l	1.65 $\pm$ 0.18	3	2.04 $\pm$ 0.33	3	0.1369
FGF23	pg / ml	131.1 $\pm$ 45.5	3	330.0 $\pm$ 49.7	3	0.0069 **
$\alpha$ -Klotho	pg / ml	2005.9 $\pm$ 1342.1	4	1873.0 $\pm$ 1016.5	4	0.8797
Osmolality	mosmol/kg	289.2 $\pm$ 11.7	5	288.1 $\pm$ 5.6	7	0.8369
CaSR	ng / ml	2.17 $\pm$ 0.98	5	2.03 $\pm$ 0.78	7	0.7816

**Table S2: Organ weights of 6 and 18-month-old animals. WT vs. KO, mean ± SD, two-tailed**

T-test.

<b>6-month-old animals</b>						
<b>Organ</b>	<b>Unit</b>	<b>WT</b>	<b>N</b>	<b>KO</b>	<b>N</b>	<b>p-value</b>
Kidney	mg	235.0 ± 32.3	7	232.9 ± 23.8	7	0.8899
Liver	mg	1332.2 ± 134.2	8	1445.6 ± 190.9	7	0.2016
Stomach	mg	339.4 ± 86.8	8	444.6 ± 256.8	7	0.2938
Spleen	mg	88.1 ± 31.3	8	99.1 ± 34.3	6	0.5467
Heart	mg	148.8 ± 31.0	8	145.4 ± 17.7	6	0.8144
<b>18-month-old animals</b>						
Kidney	mg	313.1 ± 37.6	6	313.0 ± 12.9	4	0.9950
Liver	mg	2294.1 ± 461.2	6	2399.8 ± 107.9	4	0.6703
Stomach	mg	846.8 ± 372.0	6	738.8 ± 247.6	4	0.6268
Spleen	mg	129.1 ± 52.6	6	101.6 ± 24.8	4	0.3637
Heart	mg	201.8 ± 20.4	5	231.9 ± 8.4	4	0.0285 *

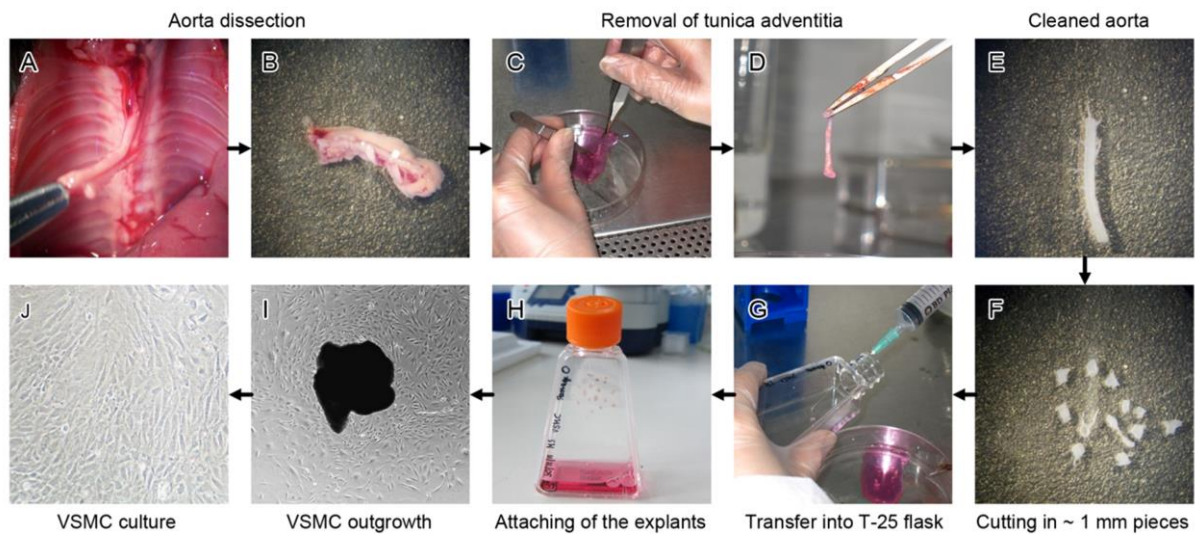


**Figure S1: Generation of explant derived aortic VSMC.** **A:** The thoracic aorta is dissected from the spine and **B:** removed to a Petri dish filled with sterile isolation medium where **C and D:** the vessel is cleared from tunica adventitia by gently pulling / scraping the connective tissue until **E:** only the semi-translucent tunica media remains. **F:** The vessel is then cut into small (ca. 1 mm) pieces that are then **G:** transferred into a T-25 cell culture flask by the use of a hypodermic needle. **H:** The flask is kept in an upright position at 37 °C for 10–15 minutes so that the explants are not in contact with medium and can attach firmly to the surface of the flask. 5 ml isolation medium is added, and the explants are kept at 37 °C / 95 % relative humidity (rh) / 5 % CO<sub>2</sub> for ca. 7 days after which the medium is changed. **I:** VSMC will start to grow out of the explants. **J:** After ca. 2-3 weeks, the explants are removed and the VSMC passaged to generate a monolayer of cells.

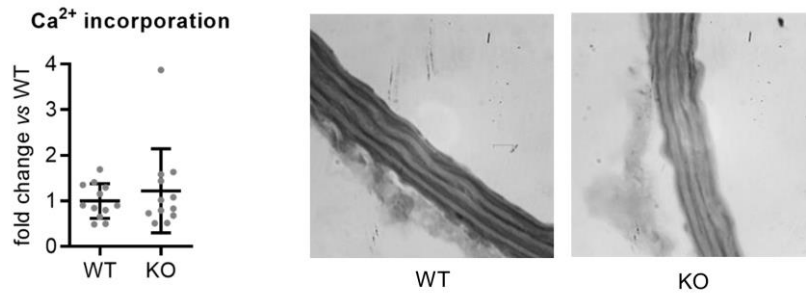


**Figure S2: *Ex vivo* aortic calcification.** Graph: Quantification of Ca<sup>2+</sup> deposition in WT and KO aortas of 3-month-old mice. Mean±SD. Pictures: Alizarin Red S stainings of thoracic aorta sections from 12-month-old WT and KO animals incubated for 10 days in the presence of medium containing 1.8 mM Ca<sup>2+</sup> and 3 mM Pi.

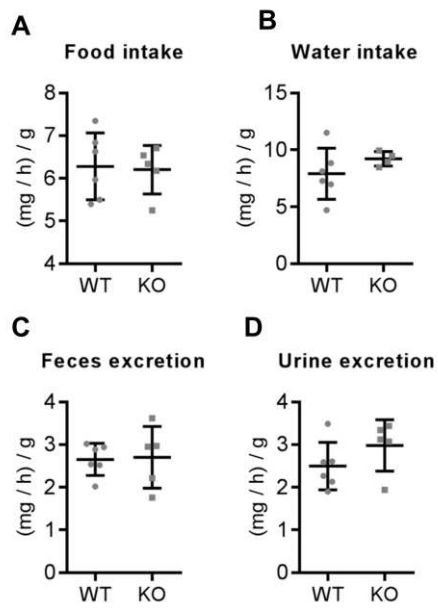


**Figure S3: Metabolic cage studies of WT and KO mice.** **A:** Food intake, **B:** Water intake, **C:** Feces excretion, **D:** Urine excretion. Data are shown as consumption (in mg) per h per g bodyweight. Mean $\pm$ SD.

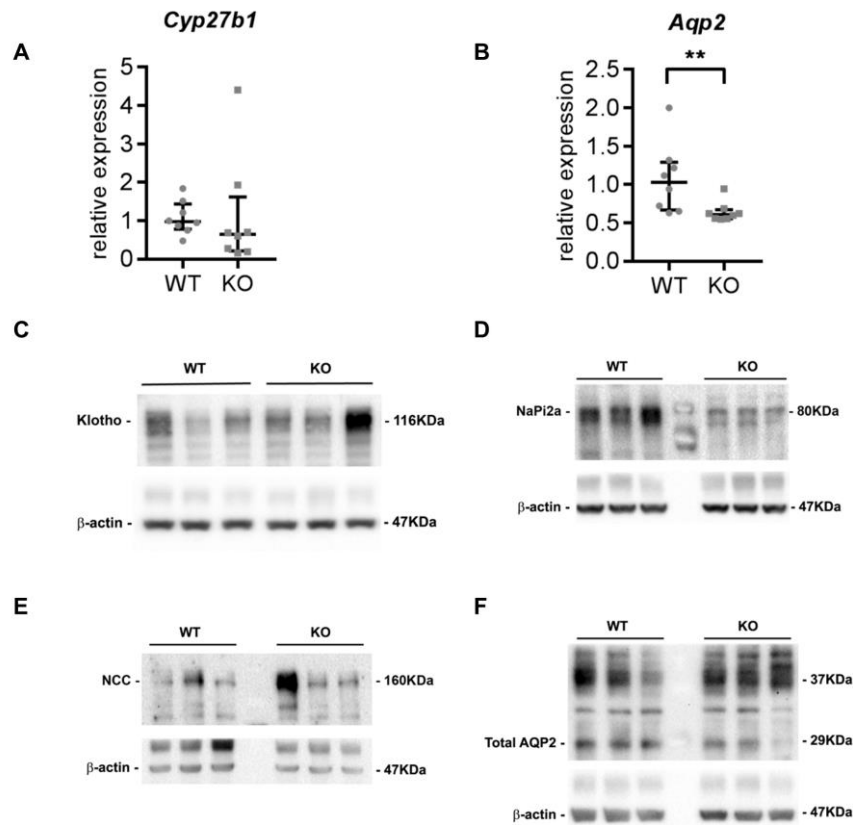


**Figure S4: Supplemental kidney mRNA and protein expression. A:** *Cyp27b1*, and **B:** *Aqp2* mRNA expression levels relative to calibrator (mean  $\Delta$ CT WT). Representative Western blots showing **C:** Klotho, **D:** NaPi2a, **E:** NCC, **F:** AQP2 expression in kidneys from WT and KO mice.

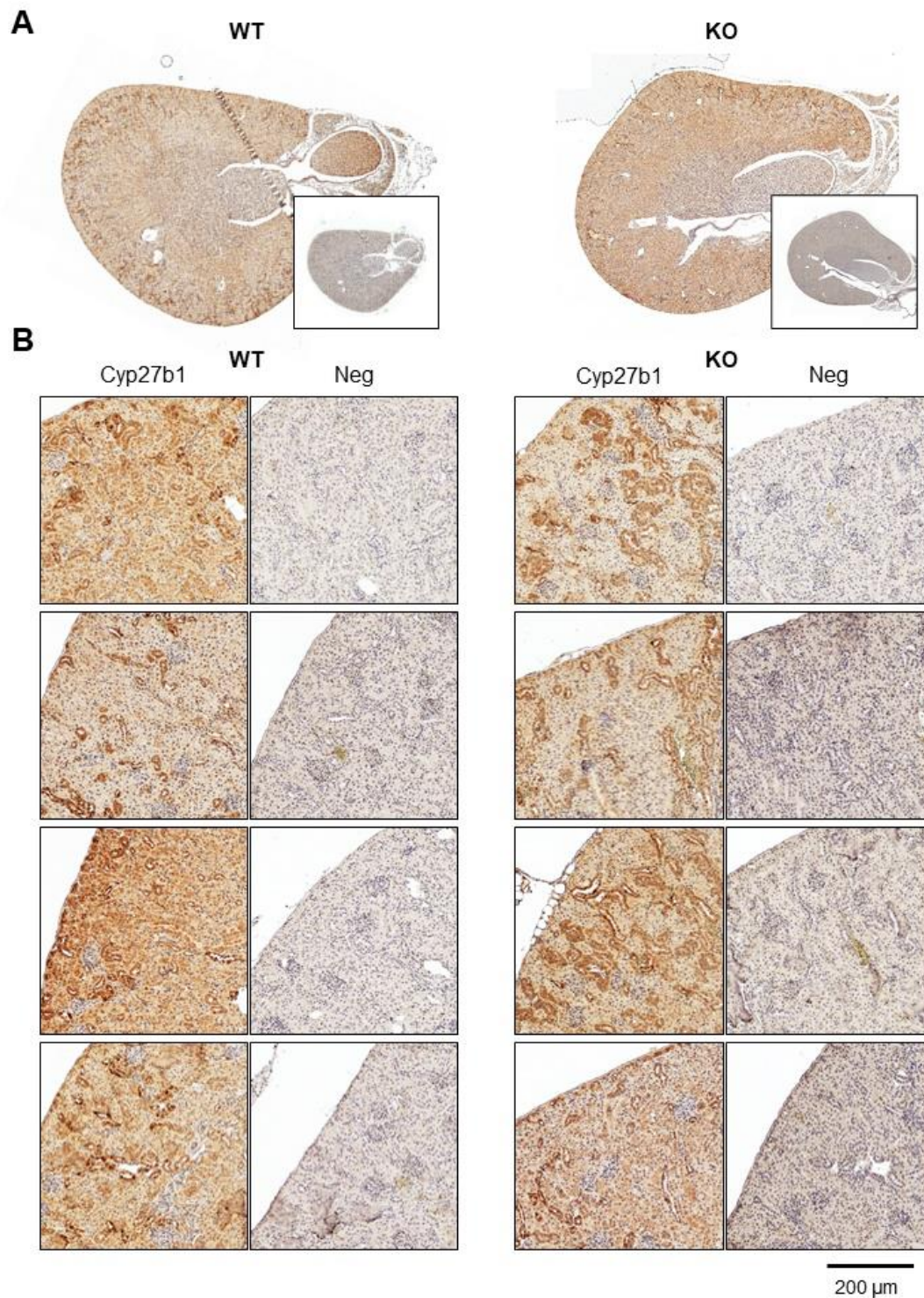


**Figure S5: Immunohistochemistry stainings of Cyp27b1 in kidneys of WT and KO mice.** Stainings were performed as described in the methods section for Cyp27b1 using the LSBio (Seattle, USA) rabbit anti-Cyp27b1 antibody at 1:1000 dilution. **A:** Overview of representative whole kidney sections stained for Cyp27b1. Insert: negative control. **B:** Cortex of N=4 WT and KO kidneys stained for Cyp27b1 and respective negative controls.



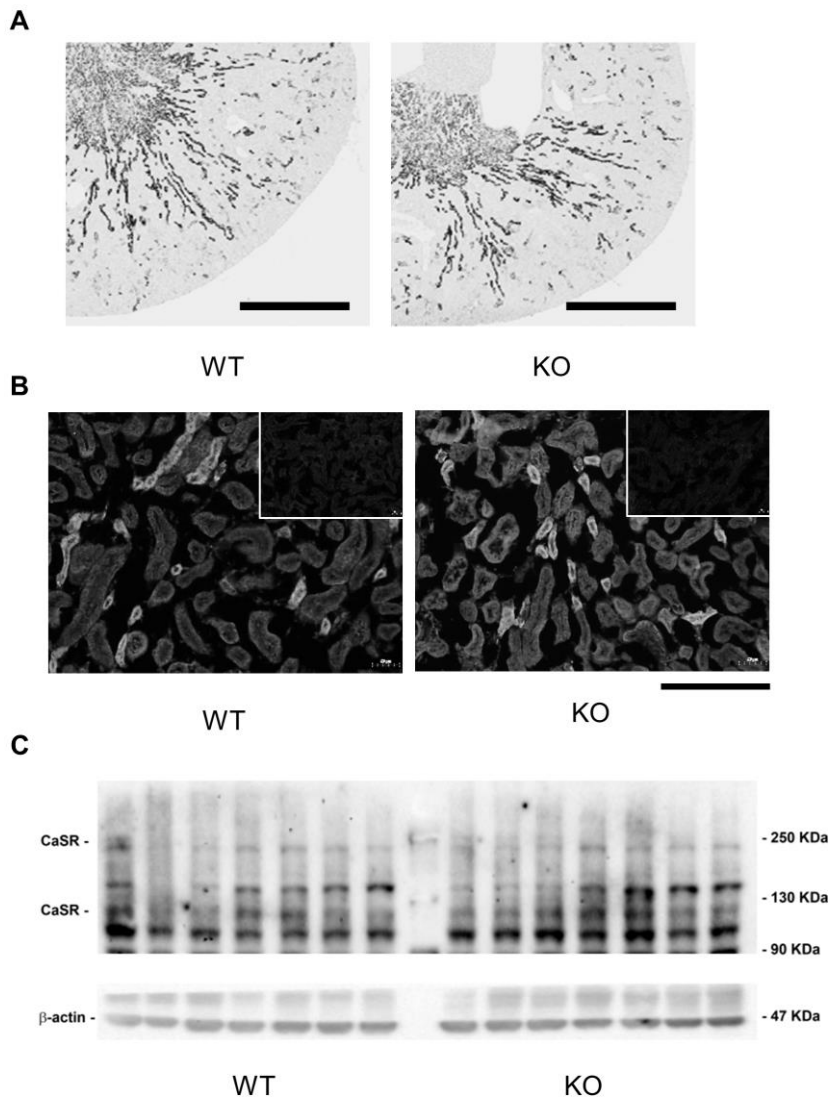


**Figure S6: Supplemental kidney CaSR expression data and representative images from Figure 3.** **A:** immunohistochemistry of CaSR expression pattern in WT and KO kidney sections. Scale bar = 1 mm. **B:** immunofluorescence analysis of CaSR expression levels in WT and KO kidneys used for quantitative immunofluorescence analysis. Scale bar = 200 μm. **C:** representative Western blot for CaSR in the kidney (~120-150 kDa: monomer; 250 kDa: dimer).



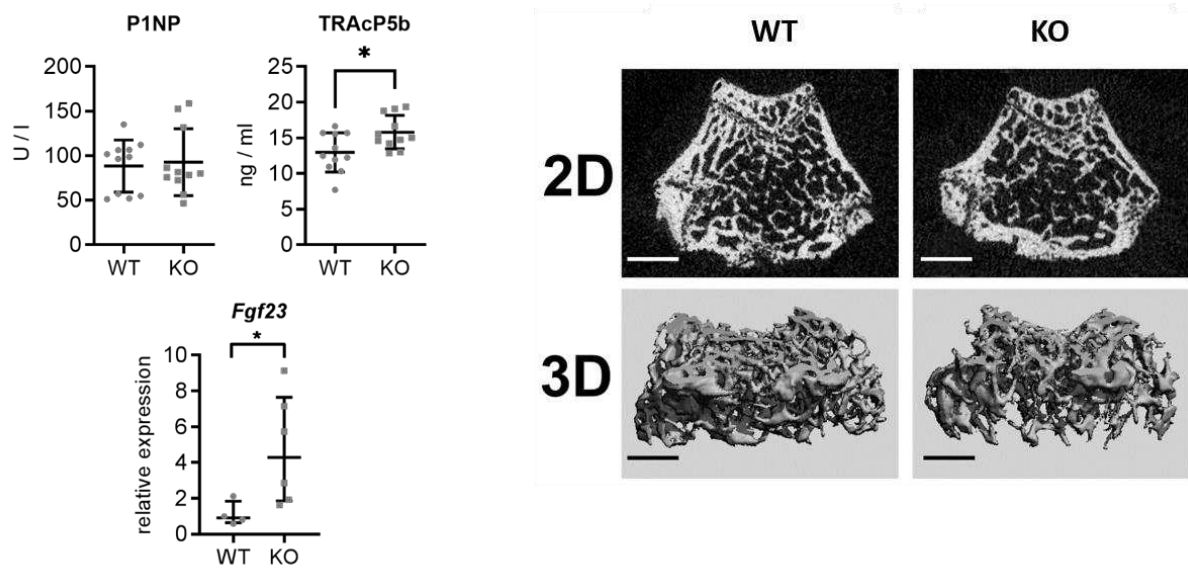


**Figure S7: Plasma levels of bone metabolism markers procollagen type 1 (P1NP) and Tartrate-resistant acid phosphatase 5b (TRAcP5b), Fgf23 mRNA expression in bone, and  $\mu$ CT.** Bone metabolism markers: \*  $p < 0.05$ , two tailed T-test; measured in male and female mice. RT-qPCR: \*  $p < 0.05$ , Mann-Whitney test.  $\mu$ CT: representative 2-dimension (2D) radiographs and 3-dimension (3D) reconstructed images from distal femurs of 3 months old KO and WT (control) littermates. The 2D radiographs were taken 100  $\mu$ m below the growth plate. Scale bar: 400  $\mu$ m

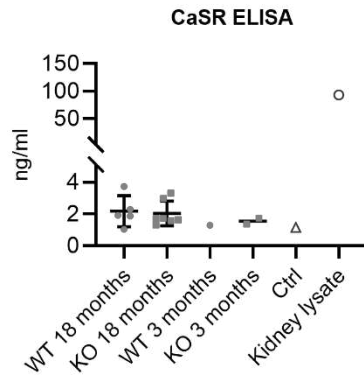


**Figure S8: Serum levels of “soluble” CaSR / CaSR fragment.** N = 5 (WT, 18 months), N = 7 (KO, 18 months), N = 3 (WT, 3 months), and N = 3 (KO, 3 months). Three of the 3-month samples, (2 WT, 1 KO) were below the detection range and are thus not included in the graph. An additional serum sample of a genetically non-modified 14 month-old mouse (“Ctrl”) was added for reference, which had a comparable level of CaSR in the serum. Finally, a sample of 100 mg / ml kidney lysate from a genetically non-modified mouse was tested as positive control.